

# Oceanic emissions of dimethyl sulfide and methanethiol and their contribution to sulfur dioxide production in the marine atmosphere

Gordon A. Novak<sup>1,a</sup>, Delaney B. Kilgour<sup>1</sup>, Christopher M. Jernigan<sup>1</sup>, Michael P. Vermeuel<sup>1,b</sup>, and Timothy H. Bertram<sup>1</sup>

5 <sup>1</sup> Department of Chemistry, University of Wisconsin – Madison, Madison, WI 53706, USA

<sup>a</sup> Now at Cooperative Institute for Research in Environmental Sciences, University of Colorado Boulder, Boulder, CO 80309, USA and National Oceanic and Atmospheric Administration (NOAA) Chemical Sciences Laboratory (CSL), Boulder, CO 80305, USA

<sup>b</sup> Now at Department of Soil, Water, and Climate, University of Minnesota – Twin Cities, St. Paul, MN 55108, USA

10 *Correspondence to:* Timothy H. Bertram (timothy.bertram@wisc.edu)

**Abstract.** Oceanic emissions of dimethyl sulfide ( $\text{CH}_3\text{SCH}_3$ , DMS) have long been recognized to impact aerosol particle composition and size, the concentration of cloud condensation nuclei (CCN), and Earth's radiation balance. The impact of oceanic emissions of methanethiol ( $\text{CH}_3\text{SH}$ , MeSH), which is produced by the same oceanic precursor as DMS, on the volatile sulfur budget of the marine atmosphere is largely unconstrained. Here we present direct flux measurements of MeSH oceanic  
15 emissions using the eddy covariance (EC) method with a high-resolution proton-transfer-reaction time-of-flight mass spectrometer (PTR-ToFMS) detector and compare them to simultaneous flux measurements of DMS emissions from a coastal ocean site. Campaign mean mixing ratios of DMS and MeSH were 72 ppt (28-90 ppt interquartile range) and 19.1 ppt (7.6-24.5 ppt interquartile range) respectively. Campaign mean emission fluxes of DMS ( $F_{\text{DMS}}$ ) and MeSH ( $F_{\text{MeSH}}$ ) were 1.13 ppt  $\text{m s}^{-1}$  (0.53-1.61 ppt  $\text{m s}^{-1}$  interquartile range) and 0.21 ppt  $\text{m s}^{-1}$  (0.10-0.31 ppt  $\text{m s}^{-1}$  interquartile range) respectively. Linear  
20 least squares regression of observed MeSH and DMS flux indicates the emissions are highly correlated with each other ( $R^2 = 0.65$ ) over the course of the campaign, consistent with a shared oceanic source. The campaign mean DMS to MeSH flux ratio ( $F_{\text{DMS}}:F_{\text{MeSH}}$ ) was  $5.5 \pm 3.0$  calculated from the ratio of 304 individual coincident measurements of  $F_{\text{DMS}}$  and  $F_{\text{MeSH}}$ . Measured  $F_{\text{DMS}}:F_{\text{MeSH}}$  was weakly correlated ( $R^2 = 0.15$ ) with ocean chlorophyll concentrations, with  $F_{\text{DMS}}:F_{\text{MeSH}}$  reaching a maximum of  $10.8 \pm 4.4$  during a phytoplankton bloom period. No other volatile sulfur compounds were observed by PTR-ToFMS to  
25 have a resolvable emission flux above their flux limit of detection or to have a gas phase mixing ratio consistently above their limit of detection during the study period, suggesting DMS and MeSH are the dominant volatile organic sulfur compounds emitted from the ocean at this site.

The impact of this MeSH emission source on atmospheric budgets of sulfur dioxide ( $\text{SO}_2$ ) was evaluated by implementing observed emissions into a coupled ocean-atmosphere chemical box model using a newly compiled MeSH oxidation  
30 mechanism. Model results suggest that MeSH emissions lead to afternoon instantaneous  $\text{SO}_2$  production of 2.5 ppt  $\text{hr}^{-1}$ , which results in a 43% increase in total  $\text{SO}_2$  production compared to a case where only DMS emissions are considered and accounts for 30% of the instantaneous  $\text{SO}_2$  production in the marine boundary layer at the mean measured  $F_{\text{DMS}}$  and  $F_{\text{MeSH}}$ . This

contribution of MeSH to SO<sub>2</sub> production is driven by a higher effective yield of SO<sub>2</sub> from MeSH oxidation and the shorter oxidation lifetime of MeSH compared to DMS. This large additional source of marine SO<sub>2</sub> has not been previously considered in global models of marine sulfur cycling. The field measurements and modeling results presented here demonstrate that MeSH is an important contributor to volatile sulfur budgets in the marine atmosphere, and must be measured along with DMS in order to constrain marine sulfur budgets. This large additional source of marine reduced sulfur from MeSH will contribute to particle formation and growth and CCN abundance in the marine atmosphere, with subsequent impacts on climate.

## 1 Introduction

Dimethyl sulfide (CH<sub>3</sub>SCH<sub>3</sub>, DMS) emissions from the ocean are the most abundant source of reduced sulfur to the marine atmosphere (Andreae, 1990; Bates et al., 1987b, 1992; Carpenter et al., 2012). The role of DMS as a driver of cloud condensation nuclei (CCN) production, which ultimately impacts Earth's radiative budget in the marine atmosphere, has been studied extensively (Bates et al., 1987a; Carslaw et al., 2013; Charlson et al., 1987; Quinn and Bates, 2011). The oxidation of DMS in the atmosphere ultimately leads to the production of methane sulfonic acid (CH<sub>3</sub>SO<sub>3</sub>H, MSA) and sulfur dioxide (SO<sub>2</sub>) which can be further oxidized to sulfuric acid (H<sub>2</sub>SO<sub>4</sub>), contributing to particle formation and growth (Clarke et al., 1998; Hoffmann et al., 2016; Schobesberger et al., 2013; Sipila et al., 2010). Direct observations and mechanistic understanding of the intermediate products in the oxidation of DMS are limited, leading to large variability in estimates of SO<sub>2</sub> yields (31 – 98%), where SO<sub>2</sub> is a precursor to sulfuric acid (H<sub>2</sub>SO<sub>4</sub>) and non-sea salt sulfate aerosol (*nss-SO<sub>4</sub><sup>2-</sup>*) (Faloona, 2009; Hoffmann et al., 2016). Previous efforts to constrain the total budget of SO<sub>2</sub> in the marine boundary layer (MBL) have required assigning a near 100% yield of SO<sub>2</sub> from DMS oxidation (Faloona et al., 2009). A 100% yield of SO<sub>2</sub> appears inconsistent with known production of MSA from DMS oxidation and with results from multiple laboratory studies (Faloona, 2009). The high yield of SO<sub>2</sub> from DMS necessary for closure of the SO<sub>2</sub> budget in that study prompted speculation on the existence of other unknown marine sulfur species which could contribute to SO<sub>2</sub> production (Gray et al., 2011). Existence of other marine contributors to SO<sub>2</sub> production would serve to reduce the implied SO<sub>2</sub> yield from DMS and would potentially bring that yield closer to the 40-80% range typically determined in laboratory and modeling studies (Gray et al., 2011). Implementation of oceanic MeSH emissions and oxidation to SO<sub>2</sub> in chemical transport models would result in an increase in sulfuric acid production with subsequent impacts on new particle formation and growth and CCN abundance.

### 1.1 DMS and MeSH oceanic production

Both DMS and the volatile reduced sulfur molecule methanethiol (CH<sub>3</sub>SH, MeSH) are produced in seawater from the same precursor metabolite, dimethylsulfoniopropionate (DMSP) (Kiene and Linn, 2000a). Bacterial cleavage of dissolved DMSP (DMSP<sub>d</sub>) primarily produces dissolved DMS (DMS<sub>d</sub>), and DMSP demethylation or demethiolation produces dissolved MeSH (MeSH<sub>d</sub>) (Yoch, 2002). MeSH<sub>d</sub> is the dominant product of DMSP<sub>d</sub> consumption with a total yield on the order of 75%, compared to an approximately 10% yield of DMS<sub>d</sub> (Kettle et al., 2001; Kiene and Linn, 2000b, 2000a). The

bacteria *Pelagibacter* HTCC1062 has been shown to simultaneously produce both DMS and MeSH, where the allocation  
65 between products may be related to the available supply of DMSP, with DMS production enhanced when the supply of DMSP  
exceeded the cellular demand for sulfur (Sun et al., 2016). While yields of MeSH<sub>d</sub> are generally higher compared to DMS<sub>d</sub>,  
MeSH<sub>d</sub> is also more rapidly consumed by heterotrophic bacteria and phytoplankton, resulting in significantly faster turnover  
times (hours for MeSH<sub>d</sub>, days for DMS<sub>d</sub>) and lower steady state dissolved concentrations (Kiene, 1996). Both MeSH<sub>d</sub> and  
70 DMS<sub>d</sub> are persistently supersaturated in the dissolved phase resulting in ventilation to the atmosphere (Kettle et al., 2001; Lee  
and Brimblecombe, 2016). Surface ocean concentrations of DMS<sub>d</sub> have been measured extensively and are on the order of 1-  
7 nM with higher values in the summer (Lana et al., 2011). This extensive collection of measurements has permitted the  
development of global climatologies of DMS<sub>d</sub> and emission fluxes for implementation into global chemical transport models  
(Galí et al., 2018; Lana et al., 2011). In contrast, measurements of MeSH<sub>d</sub> are sparse. Underway measurements from a transect  
75 of the Atlantic in September and October of 1998 showed a mean MeSH<sub>d</sub> of  $0.39 \pm 0.34$  nM and a maximum of 1.7 nM (Kettle  
et al., 2001). Mean MeSH<sub>d</sub> during that study was approximately 20% of DMS<sub>d</sub>. In the Baltic Sea, mean MeSH<sub>d</sub> was  $0.16 \pm$   
 $0.12$  nM compared to  $2.6 \pm 1.6$  nM for DMS<sub>d</sub> (Leck and Rodhe, 1991). MeSH emission fluxes were estimated to be 10% of  
DMS in that study. Significant variability in DMS<sub>d</sub> to MeSH<sub>d</sub> ratios were observed in those studies, emphasizing the need for  
more detailed study of the biogeochemical factors that control relative consumption and production of DMS<sub>d</sub> and MeSH<sub>d</sub>.

## 1.2 Atmospheric Fate of DMS

80 Once emitted to the atmosphere, DMS is oxidized by hydroxyl (OH), nitrate (NO<sub>3</sub>), chlorine (Cl), and bromine oxide (BrO)  
radicals to produce lower volatility oxidized products which can contribute to aerosol particle formation and growth (Bates et  
al., 1987a; Charlson et al., 1987; Quinn and Bates, 2011). Gas phase mixing ratios of DMS in the MBL are typically on the  
order of 50 – 600 ppt, with higher concentrations generally associated with regions of high phytoplankton abundance, and with  
diel maxima at night when oxidative loss is at a minimum (Kettle et al., 2001; Kettle and Andreae, 2000; Kim et al., 2017;  
85 Lana et al., 2011; Lawson et al., 2020; Sciare et al., 2000). Oxidation by OH, thought to be the largest loss pathway, proceeds  
either through OH addition or hydrogen abstraction. OH addition produces MSA, methane sulfinic acid (MSIA), dimethyl  
sulfoxide (DMSO), and SO<sub>2</sub>, while H-abstraction is traditionally thought to primarily produce SO<sub>2</sub> (Barnes et al., 2006; Conley  
et al., 2009; Hoffmann et al., 2016). The branching fraction of the OH oxidation channels is highly temperature dependent  
with H-abstraction favored at higher temperatures (~70% at 298 K). The DMS H-abstraction product rapidly produces the  
90 methylthiomethyl peroxy radical (MTMP, CH<sub>3</sub>SCH<sub>2</sub>OO) following recombination with atmospheric oxygen. Until recently it  
was thought that MTMP primarily participates in further bimolecular reactions with the hydroperoxyl radical (HO<sub>2</sub>), nitric  
oxide (NO), or other peroxy radicals (RO<sub>2</sub>) which efficiently produce the methyl thiyl radical (CH<sub>3</sub>S·) and ultimately SO<sub>2</sub>  
(Barnes et al., 2006; Hoffmann et al., 2016). Theoretical and laboratory studies have shown that MTMP can also undergo a  
series of intramolecular hydrogen shift rearrangements and additions of O<sub>2</sub> to form the stable product hydroperoxymethyl  
95 thioformate (HPMTF; HOOCH<sub>2</sub>SCHO) at a rate that is competitive with bimolecular reactions (Berndt et al., 2019; Wu et al.,  
2015). HPMTF has been shown to be globally ubiquitous in the marine boundary layer from airborne observations (Veres et

al., 2020) and at a coastal ocean ground site (Vermeuel et al., 2020). Global chemical transport modelling shows that 46% of emitted DMS goes on to form HPMTF (Novak et al., 2021). The atmospheric fate of HPMTF is an active topic of research but ambient observations show that dry deposition to the ocean surface is a significant loss term (lifetime ~30 hours, (Vermeuel et al., 2020)) and that HPMTF is efficiently lost to clouds (Novak et al., 2021; Veres et al., 2020; Vermeuel et al., 2020), resulting in a 35% decrease in global SO<sub>2</sub> production from DMS oxidation (Novak et al., 2021). These previously unconsidered loss processes for DMS derived sulfur may necessitate reevaluation of marine SO<sub>2</sub> budgets (Bandy et al., 2011; Faloon et al., 2009).

### 1.3 Atmospheric Fate of MeSH

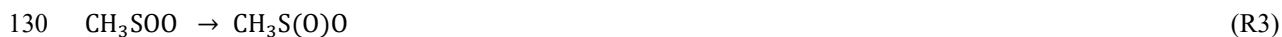
105 Comparatively little is known about the atmospheric abundance of MeSH. To date, only two ambient observations of MeSH atmospheric mixing ratios have been presented in the literature. Measurements in the remote south-west Pacific showed MeSH mixing ratios from <10 ppt to 65 ppt which were 3-36% of coincident DMS mixing ratios (Lawson et al., 2020). DMS and MeSH emission fluxes were inferred in that study from the rate of accumulation at night when oxidative loss was assumed to be zero, which showed that MeSH emission fluxes were 14-24% of the DMS flux. MeSH mixing ratios in the coastal and  
110 inshore waters west of the Antarctic peninsula were up to 3.6 ppt, which was 3% of coincident DMS (Berresheim, 1987). To our knowledge there have been no previous direct eddy covariance measurements of MeSH emission flux from the ocean.

While the bimolecular rate constants of MeSH with the primary atmospheric oxidants (OH, BrO, NO<sub>3</sub>, Cl) are known, there has been limited study on the reactive intermediates or yields of stable products from MeSH oxidation (Butkovskaya and Setser, 1999; Tyndall and Ravishankara, 1991). However, oxidation of MeSH by OH (R1) has been shown to produce the  
115 methyl thiyl radical (CH<sub>3</sub>S·) at a yield of 1.1 ± 0.2 (Tyndall and Ravishankara, 1989), providing a mechanistic link to known reactions in the DMS H-abstraction pathway (R1) (Barnes et al., 2006), as shown in the simplified reaction scheme in **Fig 1**. CH<sub>3</sub>S· production from DMS H-abstraction is the major pathway for SO<sub>2</sub> production from DMS, and the reactions of CH<sub>3</sub>S· are therefore well studied (Barnes et al., 2006). Other studies have shown that the reaction of MeSH with OH occurs primarily at the S-H group (0.87 ± 0.03) forming CH<sub>3</sub>S·, with a minor channel of H-abstraction from the methyl group (0.13 ± 0.03)  
120 (Butkovskaya and Setser, 2021). Recent ab initio/RKGM calculations determined the CH<sub>3</sub>S· yield from MeSH + OH at 298 K and 760 torr to be 0.98 (Mai et al., 2020). Given the slight inconsistency between the directly measured CH<sub>3</sub>S· yield of 1.1 ± 0.2 and the MeSH + OH branching fractions, we take these experiments to provide an upper and lower bound on the CH<sub>3</sub>S· yield of 0.87 and 1.1, and assume a CH<sub>3</sub>S· yield of 1 for R1 throughout this analysis.



125 CH<sub>3</sub>S· efficiently produces SO<sub>2</sub> through a series of competing reactions outlined in R2-R8 (Barnes et al., 2006; Hoffmann et al., 2016; Lucas, 2002; Mardyukov and Schreiner, 2018). As shown in R2, CH<sub>3</sub>S· experiences reversible addition of O<sub>2</sub> producing a methyl thiyl peroxy radical (CH<sub>3</sub>SOO) which can then undergo a series of unimolecular reactions (R3-R4) to efficiently produce SO<sub>2</sub>.





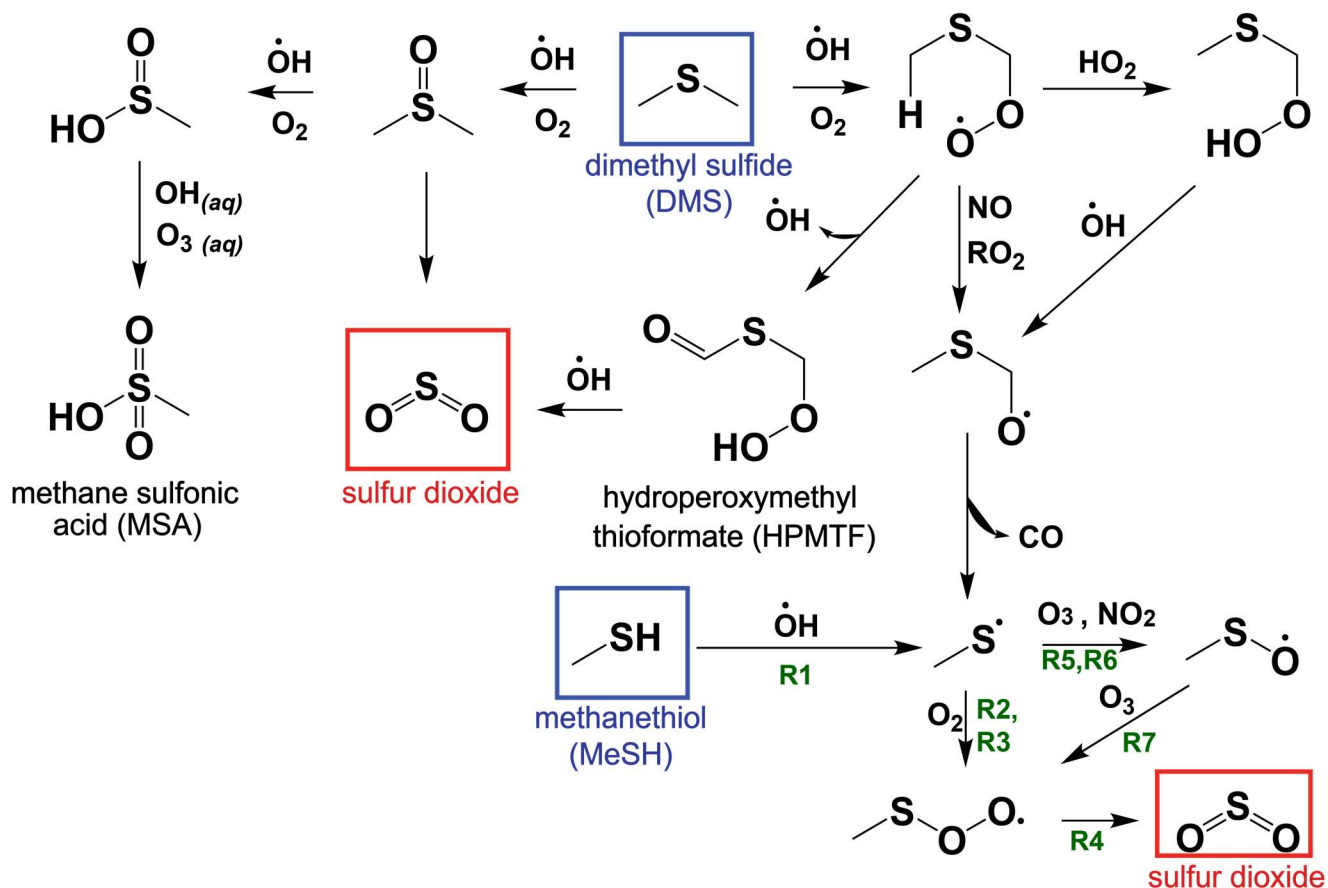
Bimolecular reactions of  $\text{CH}_3\text{S}\cdot$  with  $\text{O}_3$  and  $\text{NO}_2$  can also occur forming  $\text{CH}_3\text{SO}$  (R5-R6).  $\text{CH}_3\text{SO}$  primarily proceeds to react with  $\text{O}_3$  (R7) forming  $\text{CH}_3\text{S(O)O}$  which links back to the  $\text{SO}_2$  producing channel through R4.



A minor (~1% at open ocean  $\text{O}_3$  mixing ratios of ~20 ppb) non- $\text{SO}_2$  producing reaction pathway from  $\text{CH}_3\text{S(O)O} + \text{O}_3$  (R8) can also occur to produce  $\text{CH}_3\text{SO}_3$  which can react further to produce  $\text{SO}_3$  and MSA (Barnes et al., 2006).



140 The atmospheric yield of  $\text{SO}_2$  from the oxidation of MeSH by OH under low  $\text{NO}_x$  was recently reported as 0.98 based on modeling results constrained by a laboratory oxidation study, which is in good agreement with the efficient production of  $\text{SO}_2$  from MeSH proposed in our reaction scheme (Chen et al., 2021). We exploit this link between MeSH oxidation by OH and known DMS oxidation chemistry to develop a MeSH oxidation mechanism for implementation into a 0-D chemical box model as described further in the subsequent text. A simplified reaction diagram for the gas phase oxidation of DMS and MeSH is  
145 shown in Fig 1. The full set of reactions with rate equations are provided in **Table S1**.



150

**Figure 1.** A simplified reaction scheme for the gas phase oxidation of dimethyl sulfide (DMS) and methanethiol (MeSH) that focuses on pathways to SO<sub>2</sub> production. Reactions R1 through R7 described in Section 1.3 are labelled with green text on the schematic. Other chemical pathways including oxidation by halogens and most condensed phase reactions of DMS and its oxidation products are not shown in this simplified schematic. Refer to Table S1. for a complete list of reactions and rate equations as implemented in this work.

#### 1.4 Study Overview

Here we present eddy covariance (EC) flux measurements of DMS and MeSH emissions at a coastal ocean site using a high sensitivity Vocus PTR-TOF for detection (Krechmer et al., 2018). Results from this study show that emission fluxes of DMS  
 155 ( $F_{\text{DMS}}$ ) and MeSH ( $F_{\text{MeSH}}$ ) were well correlated ( $R^2=0.65$ ) and that  $F_{\text{MeSH}}$  is a significant contributor to marine sulfur emissions (mean  $F_{\text{MeSH}} = 0.21 \text{ ppt m s}^{-1}$ , compared to mean  $F_{\text{DMS}} = 1.13 \text{ ppt m s}^{-1}$ ). The average ratio of individual DMS to MeSH flux ( $F_{\text{DMS}}:F_{\text{MeSH}}$ ) measurements for the full campaign was  $5.5 \pm 3.0$ . We assess the impact of the observed large MeSH emission flux on production of SO<sub>2</sub> in the marine atmosphere through a coupled ocean flux -atmospheric chemistry 0-D box model with a newly compiled MeSH oxidation mechanism. Modeling results suggest that MeSH contributes approximately 30% of  
 160 instantaneous afternoon SO<sub>2</sub> production ( $P_{\text{SO}_2}$ ). Together these results show that MeSH emissions are an important contributor

to sulfur budgets in the marine atmosphere and further field studies and laboratory oxidation mechanism investigations are warranted. 2 Experimental Methods

## 2.1 Scripps Pier Flux Experiment Overview

165 Measurements of DMS and MeSH gas phase mixing ratios and EC flux were made continuously from the end of the Ellen  
Browning Scripps Memorial Pier (hereon SIO Pier) at the Scripps Institution of Oceanography in La Jolla, CA, USA during  
September 2019. The SIO Pier is 330 m long and extends over 100 m beyond the wave breaking zone. The SIO Pier site has  
been used regularly for EC studies of ocean-atmosphere trace gas exchange (Kim et al., 2014; Novak et al., 2020; Porter et al.,  
2018; Vermeuel et al., 2020). The SIO Pier experiences a characteristic sea-breeze circulation pattern during summer where  
winds are from the ocean at moderate windspeeds ( $0-6 \text{ m s}^{-1}$ ) during daytime and are from land at night, which limits nighttime  
170 flux determinations. DMS and MeSH were detected with a latest generation Vocus PTR-TOF (Vocus) instrument  
(TOFWERK, Aerodyne), with an HTOF mass analyzer (resolution *ca*  $5000 \text{ m}/\Delta m$  for DMS and MeSH) (Krechmer et al.,  
2018). The Vocus was housed in a temperature-controlled trailer at the end of the pier and sampled through a 19 m long PFA  
inlet (0.625 cm i.d.) enclosed in an opaque housing to prevent photochemistry in the sampling line. The inlet was pumped at  
22 slpm which maintained turbulent flow and short residence times in the sampling line (Reynolds number 4280, calculated  
175 volumetric evacuation time 1.7 s). The full inlet line was held at  $40^\circ\text{C}$  which was always above ambient temperatures to prevent  
condensation of water vapor on inlet surfaces. A bypass line through the Vocus front end subsampled from the main inlet at 5  
slpm through a PFA tee located at the instrument interface. The Vocus subsampled from this bypass at a flow rate of 100 sccm  
immediately in front of the Vocus capillary inlet into the instrument drift tube. This sampling configuration was used to reduce  
residence times in the sampling lines as much as possible (total estimated inlet and instrument residence time  $\sim 1.9 \text{ s}$ ). In  
180 addition to the main inlet line, all surfaces in contact with the ambient sample flow, including unions and valves, were  
composed of PFA or PEEK in order to minimize known surface artifacts for MeSH sampling except for one stainless-steel  
union at the Vocus subsampling point (Perraud et al., 2016). The ambient inlet sampling point was collocated with a sonic  
anemometer recording three-dimensional winds at 10 Hz (Gil HS-50). The sonic anemometer and Vocus inlet were mounted  
on a 6.1 m long boom extended beyond the end of the pier to minimize flow distortions from the pier. The inlet was mounted  
185 on the boom at a height of 13 m above the mean lower low tide level. Ocean depth below the pier sampling point was *ca.* 6 m.  
The Vocus was operated at a drift tube pressure of 1.5 mbar and an axial electric field gradient of  $41.5 \text{ V cm}^{-1}$  resulting in a  
high overall effective field strength (E/N) of 143 Td. Mass spectra were recorded at 10 Hz for the full mass range of 19-500  
 $\text{m}/Q$ . The second RF-only focusing quadrupole in the instrument was operated at an amplitude of 275 V at the start of the  
campaign before being reduced to 235 and ultimately 215 V later in the deployment. The reduced amplitude on the quadrupole  
190 increased transmission of low mass ( $<50 \text{ m}/Q$ ) ions as described by Krechmer et al., (2018). MeSH ( $\text{m}/Q$  49) transmission was  
increased by 10% at the reduced amplitude of 215 V, compared to 275 V, which was accounted for in the data processing.  
Transmission efficiency of DMS was independent of the quadrupole amplitude as its nominal mass ( $\text{m}/Q$  63) is larger than the

mass discrimination window of the quadrupole. High resolution peak fitting and integration of the mass spectra was performed in the Tofware 3.2.0 software developed by the instrument manufacturer (TOFWERK).

195 Additional ancillary measurements made continuously from the pier included O<sub>3</sub> mixing ratios, temperature, relative humidity, and incoming solar irradiance. O<sub>3</sub> mixing ratios were measured at 1-minute time resolution (POM, 2B Technologies) in line with the Vocus with a subsampling point immediately downstream of the Vocus subsampling point. Temperature and RH (Vaisala HMP110) were also measured inline downstream of the Vocus subsampling point at 1 Hz time resolution. Incoming total solar irradiance at 1 Hz time resolution (Licor LI-200R) was measured via a sensor mounted on top of the trailer housing the Vocus. Measurements of sea-surface temperature (SST), salinity, and chlorophyll are continuously collected at a 1-minute time resolution from the end of the pier from an automated shore station operated by the Southern California Coastal Ocean Observing System (Wright, 2016).

## 2.2 DMS and MeSH calibrations and limit of detections

Instrument calibration factors for DMS were determined during ambient sampling by a two-point standard addition of a DMS gas standard (Praxair, 5.08 ppm ± 5%) to the full sampling inlet every 2.5 to 4 hours. Campaign mean sensitivity to DMS was 3.9 cps ppt<sup>-1</sup>. Sensitivity to DMS was independent of RH. MeSH was not directly calibrated for during field sampling. Post campaign calibrations for MeSH were performed in the laboratory using a MeSH compressed gas standard (Airgas, 6.11 ± 5% ppm) yielding a calibration factor of 1.3 cps ppt<sup>-1</sup> for dry conditions. MeSH sensitivity was slightly humidity dependent resulting in the sensitivity at 80% RH being 11% lower than at 0% RH. Calibrations for MeSH were performed with the same 19 m sampling line and flow conditions used for ambient sampling. We expect that this reduced sensitivity for MeSH at high RH is at least partially due to reactions on inlet surfaces which is a known complication in MeSH sampling (Perraud et al., 2016). Ambient MeSH calibration factors were determined by scaling the measured in-field DMS calibration factors by the RH dependent DMS:MeSH sensitivity ratio determined from the laboratory calibrations. We note that the observed sensitivity ratio of DMS:MeSH is different from what would be predicted based on measured proton transfer rate coefficients which are approximately equal for DMS and MeSH (Williams et al., 1998), emphasizing the need for direct calibration of MeSH.

Instrument backgrounds were determined by overflowing the full inlet line with dry UHP N<sub>2</sub> at the tip of the ambient sampling point. Ambient sampling periods were subdivided into 30-minute blocks and were matched to the nearest temporal calibration and background determination point. The campaign mean, median, and interquartile range for DMS were 72.6, 49.2, and 28.0-89.8 ppt respectively. MeSH mean, median, and interquartile ranges mixing ratios were 19.1, 13.4, and 7.6-24.5 ppt. Limits of detection (LOD) at a signal-to-noise (S/N) ratio of three were 2.6 ppt for DMS and 3.6 ppt for MeSH for a 10 s averaging time following the calculation method of Bertram et al., (2011).



## 2.3 Eddy Covariance Flux Measurements

### 2.3.1 Eddy Covariance Calculation Overview

The flux ( $F$ ) of trace gas across the interface is described by Eq. 1, as a function of both the gas-phase ( $C_g$ ) and liquid phase  
225 ( $C_l$ ) concentrations and the dimensionless gas over liquid Henry's law constant ( $H$ ), where  $K_t$ , the total transfer velocity for  
the gas, encompasses all of the chemical and physical processes that govern air-sea gas exchange (Liss and Slater, 1974).

$$F = K_t(HC_l - C_g) \quad (1)$$

Both DMS and MeSH are persistently supersaturated in the liquid phase leading to an emission flux to the atmosphere (where  
a positive flux value indicates emission). Fluxes of DMS and MeSH were measured in the turbulent planetary boundary layer  
230 with the well-established eddy covariance (EC) technique, where  $F$  is calculated as the time average of the instantaneous  
covariances from the mean of vertical wind ( $w$ ) and the scalar magnitude ( $x$ , here either DMS or MeSH) as shown in Eq. 2.  
Overbars are means and primes are the instantaneous variance from the mean.  $N$  is the total number data points during the flux  
averaging period. Ambient data was subdivided into approximately 30-minute flux averaging periods for the EC flux  
calculation.

$$235 F_x = \frac{1}{N} \sum_{i=1}^N (w_i - \bar{w})(x_i - \bar{x}) = \langle w'x' \rangle \quad (2)$$

### 2.3.2 EC Flux Data Processing and Quality Control

Several standard EC data processing steps, data filters, and quality control checks were applied during flux analysis including:  
1) filtering by wind direction for periods of onshore winds (true wind direction 200-360°), 2) coordinate rotation of three-  
dimensional wind components by the planar fit method to remove unintentional tilts in the sonic mounting and account for  
240 local flow distortions (Wilczak et al., 2001), 3) application of a friction velocity ( $U_*$ ) threshold of 0.05 cm s<sup>-1</sup> to reject periods  
of low shear driven turbulence, 4) despiking of DMS and MeSH data using a mean absolute deviation filter before the EC flux  
calculation (Mauder et al., 2013), 5) linear detrending of the scalar timeseries, and 6) flux stationarity filtering with flux periods  
rejected if they were non-stationary at a 30% threshold (Foken and Wichura, 1996). Additional discussion of EC flux  
processing and quality control steps including lag time determination, spectral analysis, frequency attenuation corrections, and  
245 flux LOD determination are provided in SI. A total of 304 out of 696 flux measurement periods passed all quality control filters.  
Campaign mean flux of DMS was 1.13 ppt m s<sup>-1</sup> with a mean of individual flux period limits of detection at the 3 $\sigma$  confidence  
interval of 0.35 ppt m s<sup>-1</sup>. MeSH mean flux was 0.21 ppt m s<sup>-1</sup> with a mean flux 3 $\sigma$  LOD of 0.11 ppt m s<sup>-1</sup>.

## 2.4 Coupled ocean-atmosphere flux chemical box model

### 2.4.1 Meteorological and Chemical Constraints

250 A coupled ocean-atmosphere 0-D chemical box model was developed using the Master Chemical Mechanism (MCM) v3.3.1  
(<http://mcm.york.ac.uk>, Jenkin et al., 1997; Saunders et al., 2003) in the Framework for 0-D Atmospheric Modeling (F0AM,

Wolfe et al., 2016) with added chlorine chemistry (Riedel et al., 2014). The model was used to assess the impact of observed MeSH emissions on production of secondary marine SO<sub>2</sub>. Model ability to reproduce observed diel profiles of DMS and MeSH mixing ratios was also tested. Measured emission fluxes of MeSH and DMS are coupled into the model to set the source term for those molecules. Ambient pressure and temperature data were acquired from the NOAA National Data Buoy Center (Stations LJPC1 and LJAC1) as well as from an onsite temperature and relative humidity data logger (OM-62, Omega Engineering). Chemical constraints included coincident measurements of O<sub>3</sub> and nitryl chloride (ClNO<sub>2</sub>) measured at the same site in August 2018 (Vermeuel et al., 2020), an assumed OH profile that followed the solar cycle with a peak at 4.0 x 10<sup>6</sup> molecules cm<sup>-3</sup>, and constant concentrations of other major trace gases as listed in **Table S2**. A constant first-order dilution loss term was used with a one-day lifetime to approximate mixing out of the boundary layer. A static boundary layer height (BLH) of 500 m was assumed (Faloona et al., 2005; Stull, 1988; Wei et al., 2018). Clear sky conditions were also assumed (i.e. no heterogeneous loss from reactive uptake on cloud droplets (Vermeuel et al., 2020)). An updated oxidation mechanism for DMS and MeSH was implemented, expanding upon the default DMS oxidation scheme in the MCM v3.3.1 to include oxidation of MeSH to form CH<sub>3</sub>S· (R1) and to include HPMTF chemistry, detailed in **Table S1**. The model was allowed to spin up for two days to allow reactive intermediates to reach equilibrium, with all reported values taken from day three of the model run.

## 2.4.2 Box Model Conditions

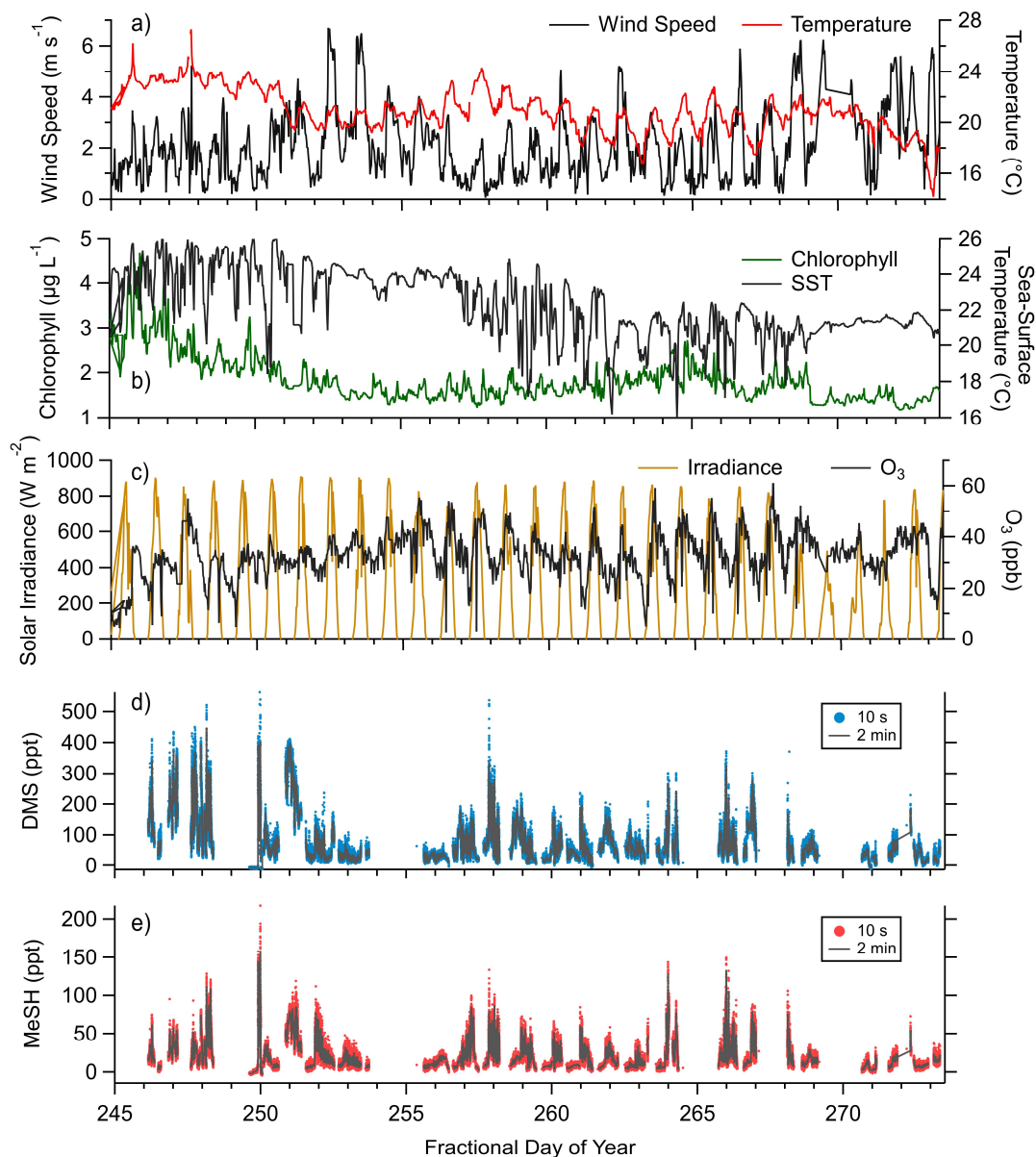
### 2.4.2.1 Pier Model Case

Two distinct model cases were developed which differ in how they treat the diel profile of  $F_{\text{DMS}}$  and  $F_{\text{MeSH}}$ . The first (termed the Pier Model Case) used the observed diel profile of  $F_{\text{DMS}}$  and  $F_{\text{MeSH}}$  at Scripps Pier to test model ability to reproduce observed diel profile of DMS and MeSH gas phase mixing ratios. Nighttime flux measurements from 23:00 to 09:00 were limited during this study due to persistent off-shore wind conditions. Instead, we apply a constant nighttime emission flux taken as the average of the 9:00-10:00 and 21:00-22:00 flux observations for DMS and MeSH. A three-hour moving mean was also applied to the observed diel flux profiles to reduce the influence of experimental variability on the model. This Pier Model Case is used in the analysis of diel profiles presented in **Section 3.4**.

### 2.4.2.2 Open Ocean Case

A second case (termed Open Ocean Model Case) was developed to provide a general assessment of the relative contribution of DMS and MeSH emissions to SO<sub>2</sub> production as described in **Section 3.5**. This Open Ocean case uses fixed values for  $F_{\text{DMS}}$  and  $F_{\text{MeSH}}$  taken as the campaign mean fluxes, rather than a variable diel profile. This case avoids the ambiguity of uncertain nighttime emission flux in the observations and better represents conditions on the open ocean where there is little diel variability in wind speed and thus emission fluxes for DMS and MeSH are expected to be relatively constant (Archer and Jacobson, 2005).

### 3 Results and Discussion



285 **Figure 2.** Campaign time series of (a) Wind speed and near surface air temperature, (b) chlorophyll concentration and sea-surface  
temperatures (SST), (c) Incoming solar irradiance (from 400-100 nm) and ozone (O<sub>3</sub>) mixing ratios, (d) mixing ratios of DMS at 10  
s and 2 minute time resolution, and (e) mixing ratios of MeSH at 10 s and 2 minute time resolution.

#### 3.1 Meteorology Overview

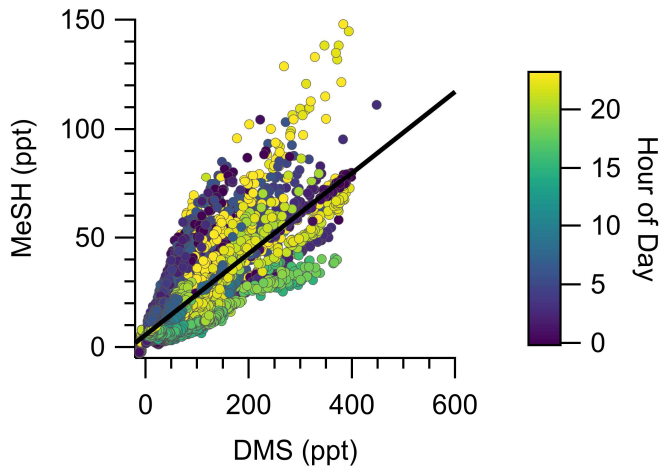
Observed meteorology and ocean physical and biogeochemical parameters showed minimal variance over the sampling period.

290 Mean sea-surface temperature during the campaign was 23.3°C (21.6 to 24.7°C interquartile range). Observed mean and

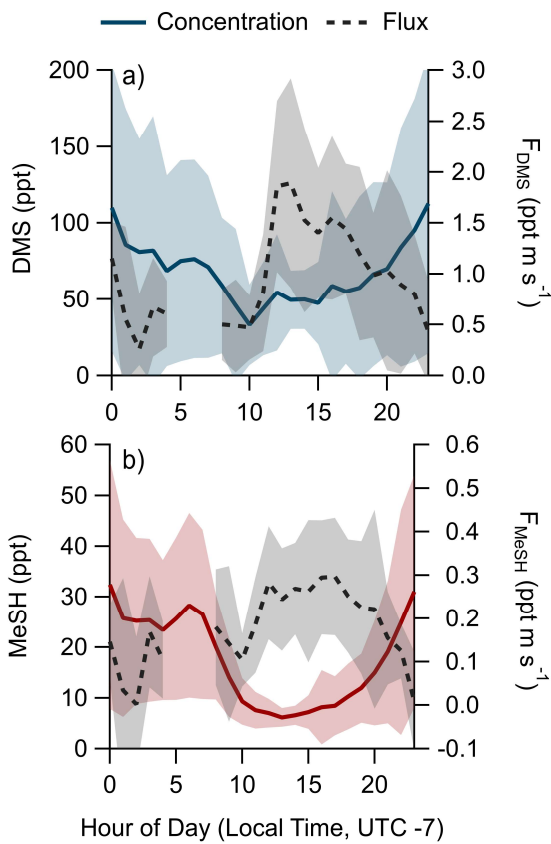
interquartile ranges of air temperatures and relative humidity were 22°C (19.5 to 23.6°C) and 79.9% (72.3 to 88.3%) respectively. Chlorophyll concentrations suggest moderate biological productivity with an observed campaign mean of 1.86  $\mu\text{g L}^{-1}$  (1.5 to 2.0  $\mu\text{g L}^{-1}$  interquartile range).  $\text{O}_3$  mixing ratios showed a clear diel pattern peaking in mid-afternoon with a campaign mean of 32.6 ppbv (27.6 to 38.9 ppbv interquartile range). Wind speeds during onshore wind periods were from 0 to 6  $\text{m s}^{-1}$ , typically peaking in late afternoon with a campaign mean of 2.8  $\text{m s}^{-1}$ . Clear sky conditions were observed for most afternoons during the study period, with total solar irradiance peaking near noon. The period from day of year (DOY) 268-271 saw occasional overcast skies during the afternoon. Light rainfall during the early morning of the DOY 271 was the only precipitation during the campaign. Morning and late evening periods showed occasional presence of marine stratocumulus clouds which drove day-to-day variability in solar irradiance during those times. The campaign timeseries of wind speed, air temperature, sea surface temperature (SST),  $\text{O}_3$  mixing ratios, solar irradiance, and DMS and MeSH mixing ratios are presented in **Fig. 2**. Gaps in the DMS and MeSH timeseries are from instrument maintenance periods, power outages at the site, and periods where the instrument was operated in an alternative sampling mode.

### 3.2 DMS and MeSH Gas Phase Mixing Ratios

The campaign mean, median, and interquartile range of DMS mixing ratios were 72.6, 49.2, and 28.0-89.8 ppt respectively. MeSH mean, median, and interquartile range mixing ratios were 19.1, 13.4, and 7.6-24.5 ppt. Maximum concentrations of DMS and MeSH during the campaign were 562 and 217 ppt respectively, for 10 s time averaged data. The correlation of observed DMS and MeSH mixing ratios at 2 minute averaging time colored by the hour of day (local time, UTC-7) of the observation are shown in **Fig. 3**. The slope of the correlation was 0.19 with a linear least squares regression coefficient ( $R^2$ ) of 0.61. The ratio of DMS:MeSH mixing ratios reaches a minimum near hours 05-07 following the build-up of MeSH overnight. Both DMS and MeSH were observed to reach a maximum in concentration at night, and minimum concentrations in the early afternoon as shown in the diel profiles in **Fig. 4**. The observed diel profile is consistent with expectations due to the significantly lower oxidative loss rate at night and has been observed in other studies (Lawson et al., 2020). MeSH varies by approximately a factor of five between its diel average maximum and minimum concentration, compared to DMS which varies by approximately less than a factor of three. The larger diel variability in MeSH is due to its approximately five times faster bimolecular rate constant with OH ( $k_{\text{OH}+\text{MeSH}} = 3.3 \times 10^{-11} \text{ cm}^3 \text{ molecule}^{-1} \text{ s}^{-1}$  at 293 K) compared to DMS ( $k_{\text{OH}+\text{DMS}} = 7.8 \times 10^{-12} \text{ cm}^3 \text{ molecule}^{-1} \text{ s}^{-1}$  at 293 K) resulting in a lifetime of MeSH to oxidation by OH during the afternoon on the order of 3 hours compared to 16 hours for DMS (for  $[\text{OH}] = 2 \times 10^6 \text{ molecule cm}^{-3}$ ). In the remote south-west Pacific Ocean, Lawson et al. (2020) measured mean DMS and MeSH mixing ratios of 208 and 18 ppt respectively, with maximum concentrations observed at night. They also found that DMS and MeSH were correlated, with a slope of 0.07 and an  $R^2$  of 0.3 over the full campaign. We observe similar mean MeSH (19.1 ppt), lower DMS (72.6 ppt), and a larger slope for the correlation of DMS and MeSH (slope = 0.19) in this study compared to the Lawson et al. (2020) observations. Still our results show general qualitative agreement with Lawson et al (2020), with both showing that atmospheric MeSH is present at a significant ratio relative to DMS.



325 **Figure 3. Correlation of DMS and MeSH mixing ratios at a 2 minute averaging time colored by hour of day of the observation. Hour of day is in local time (UTC -7). The linear least-squares best fit is plotted as the solid black line. The slope of the best fit line is 0.19 and  $R^2 = 0.61$ .**



330 **Figure 4. Hourly averaged diel profiles of observed mixing ratios and eddy covariance flux of (a) DMS and (b) MeSH. Shading represents the standard deviation of the binned hourly means. Winds were primarily from the land for hours 0 to 10, limiting air-sea flux measurement during those times.**

### 3.3 DMS and MeSH Emission Flux

A total of 304 valid quality-controlled flux averaging periods were measured during the campaign. Campaign mean emission fluxes of  $F_{\text{DMS}}$  and  $F_{\text{MeSH}}$  were 1.13 ppt m s<sup>-1</sup> (0.53 – 1.61 ppt m s<sup>-1</sup> interquartile range) and 0.21 ppt m s<sup>-1</sup> (0.10 – 0.31 ppt m s<sup>-1</sup> interquartile range) respectively. Both  $F_{\text{DMS}}$  and  $F_{\text{MeSH}}$  reached a steady maximum between hour of day 10 to 17 as shown in **Fig. 4** which corresponds to the typical period of sustained peak wind speed. The magnitude of both  $F_{\text{DMS}}$  and  $F_{\text{MeSH}}$  were found to increase with wind-speed as shown in **Fig 5**, following expectations for supersaturated species at moderate wind speeds where flux magnitude is controlled by physical transfer terms (Carpenter et al., 2012; Huebert et al., 2004; Kim et al., 2017; Marandino et al., 2007). Measurement of  $F_{\text{DMS}}$  and  $F_{\text{MeSH}}$  during nighttime was limited due to persistent winds from the land at night throughout the campaign. Less than 15% of the valid flux observations were between the hours 22 – 07. Further, those nighttime flux measurements were smaller and showed high variability compared to daytime measurements. DMS and MeSH fluxes were highly correlated with each other ( $R^2 = 0.65$ ) as shown in **Fig. 6a**. Campaign mean  $F_{\text{DMS}}:F_{\text{MeSH}}$  calculated as the simple mean of the ratio of individual  $F_{\text{DMS}}$  and  $F_{\text{MeSH}}$  observations was  $5.5 \pm 3.0$ . Lawson et al. (2020) calculated the average emission flux of MeSH compared to DMS ( $F_{\text{MeSH}} / (F_{\text{MeSH}} + F_{\text{DMS}})$ ) to be between 14% - 24%, where fluxes were calculated from the nighttime accumulation of DMS and MeSH when oxidative loss was assumed to be negligible. In this study using direct eddy covariance flux measurements, we calculate the mean  $F_{\text{MeSH}} / (F_{\text{MeSH}} + F_{\text{DMS}})$  to be 16%, which compares well to the Lawson et al. (2020) result. As shown in **Fig. 6b**,  $F_{\text{DMS}}:F_{\text{MeSH}}$  is partially correlated ( $R^2 = 0.15$ ) with ocean chlorophyll concentrations. The timeseries of chlorophyll concentrations shown in **Fig. 2b**. shows that chlorophyll peaked at the immediate start of gas phase sampling from DOY 245-246 at *ca.* 3.5 to 4  $\mu\text{g L}^{-1}$  before declining over the course of several days to roughly constant concentrations from 1 to 2.5  $\mu\text{g L}^{-1}$  over the remainder of the campaign. The profile of chlorophyll suggests a phytoplankton bloom peak and decay was sampled in the first period of the campaign which transitioned into a roughly constant moderately biologically productive state for the remainder of the campaign.  $F_{\text{DMS}}:F_{\text{MeSH}}$  during the period of peak chlorophyll concentrations over the first three days of the campaign (DOY 245 - 247) was  $10.8 \pm 4.4$  compared to the mean ratio from the full campaign of  $5.5 \pm 3.0$ . The relative production and consumption of DMS and MeSH in seawater is known to be a complex function of the speciation and abundance of phytoplankton and bacteria as well as available organic sulfur and other biogeochemical parameters (Kiene et al., 2000; Kiene and Linn, 2000b). No other measured meteorological parameters including wind speed, SST, and solar irradiance showed a significant correlation with  $F_{\text{DMS}}:F_{\text{MeSH}}$ . The underlying cause for the correlation between  $F_{\text{DMS}}:F_{\text{MeSH}}$  and chlorophyll in our dataset is not clear without additional constraints on the ocean biochemistry. However, this result highlights that biological activity can drive variations in dissolved ratios of DMS and MeSH resulting in variability in ambient  $F_{\text{DMS}}:F_{\text{MeSH}}$  emission ratios, and that further study is needed to elucidate this mechanism and its spatiotemporal variability. Measurements during an induced mesocosm phytoplankton bloom experiment using seawater collected as SIO pier immediately before this study showed that the ratio of gas phase DMS to MeSH varied by more than a factor of five over the course of a phytoplankton bloom and decay (Kilgour et al., 2022). DMS to MeSH ratios in that study were strongly linked to changes in bacterial sulfur demand and changes in the available pool of dissolved sulfur

365 across the phytoplankton bloom and decay cycle. Sun et al., (2016) have also shown that the bacterium *Pelagibacter* produces both DMS and MeSH from DMSP, where the relative yield of products is related to the amount of excess DMSP compared to the cellular demand for sulfur for biosynthesis. While induced mesocosm blooms and incubation experiments are not fully representative of the ambient ocean, these results demonstrate the controlling role of ocean biology on  $F_{\text{DMS}}$  and  $F_{\text{MeSH}}$  and ultimately on marine  $\text{SO}_2$  production which must be better constrained through further ambient observations.

370

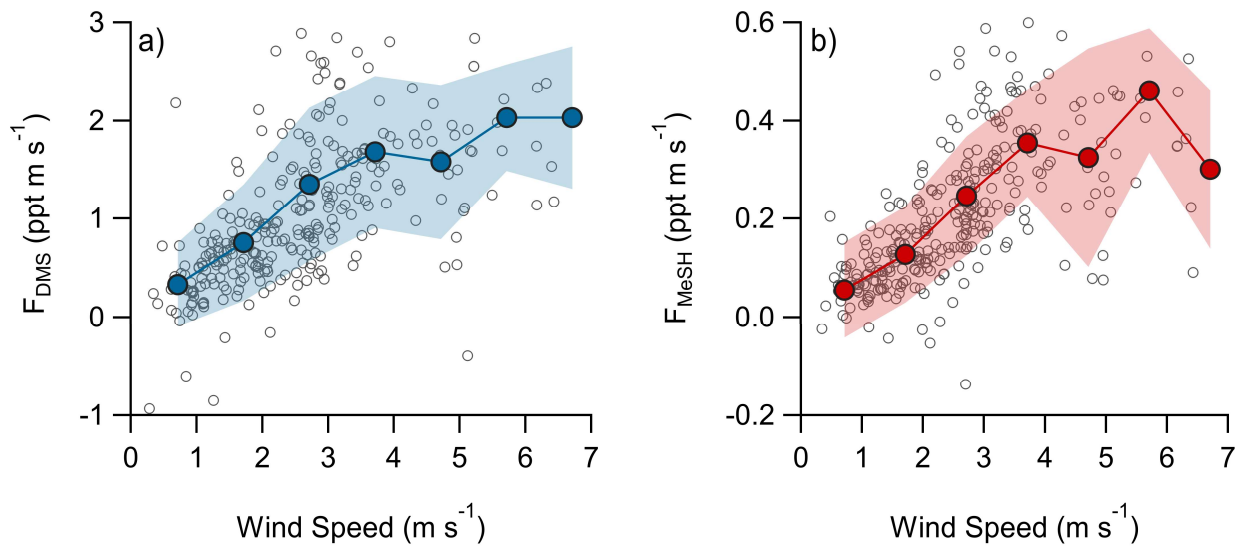
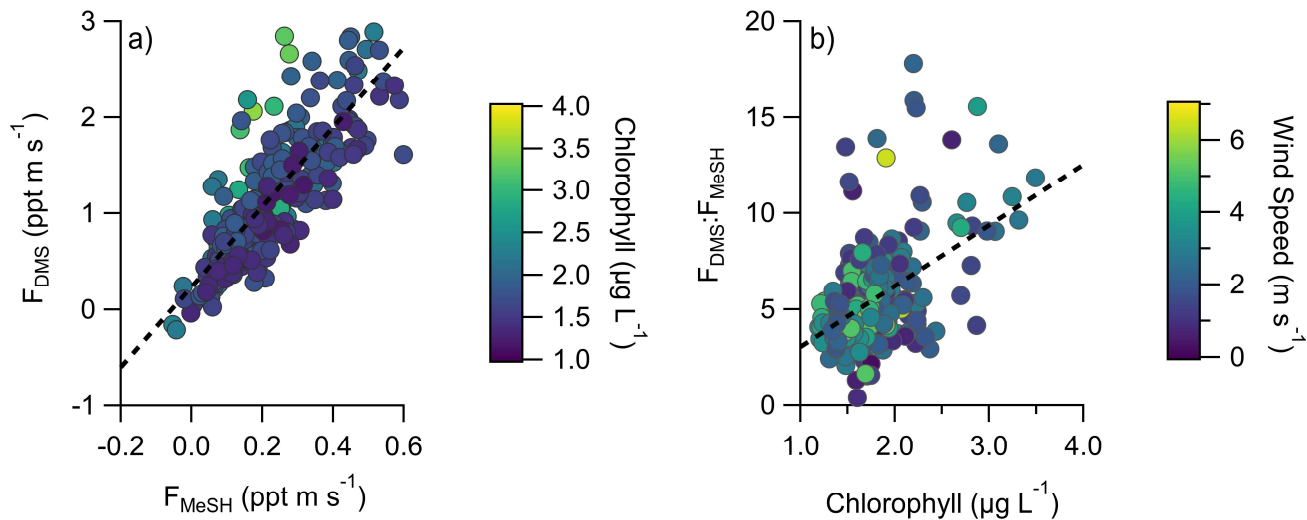


Figure 5. Flux of (a) DMS and (b) MeSH as a function of wind speed. Open circles are individual thirty-minute data points and closed circles are mean fluxes binned by wind speed at a  $1 \text{ m s}^{-1}$  bin spacing. Shaded regions are  $\pm 1\sigma$  of the binned mean.



375

Figure 6. (a) Correlation and linear-least squares regressions of measured MeSH and DMS emission fluxes ( $F_{\text{MeSH}}$  and  $F_{\text{DMS}}$  respectively). The slope of the best fit line is 4.15 and  $R^2 = 0.65$ . (b) Correlation and linear-least squares regression of the emission flux ratio of DMS to MeSH ( $F_{\text{DMS}}:F_{\text{MeSH}}$ ) with ocean chlorophyll concentrations. The slope of the best fit line is 3.15 and  $R^2 = 0.15$ . Points in (a) are colored by ocean chlorophyll concentrations and in (b) by mean wind speeds for each flux period.

### 380 3.4 Chemical Box Model Comparison to Pier Observations

We assessed the ability of the coupled ocean-atmosphere chemical box model described in Section 2.4.2 using the Pier Model Case to replicate the observed mean diel profiles of DMS and MeSH mixing ratios from the SIO pier. The model and measurement diel profiles of DMS and MeSH are shown in Fig. 7. For MeSH the model agrees with measurements to within 25% during daytime hours (10 – 21) when direct flux constraints were possible but diverges significantly at night where the model underpredicts MeSH. DMS is overpredicted by roughly 25 ppt during daytime (hours 9 to 20) in the model. Modeled DMS also shows less day-night variability in concentration, varying by a factor of 1.25 compared to observations which vary by approximately a factor of 2. The poorer model performance at night is likely related to diel changes in coastal boundary layer dynamics, including boundary layer height and advection, which are not captured in the model. As noted, nighttime emission fluxes of DMS and MeSH are poorly constrained by the EC flux measurements and may also contribute to the larger disagreement at nighttime. We expect the most informative model test case is for MeSH mixing ratios during daytime, where the MeSH emission flux is well constrained by measurements and the oxidative lifetime of MeSH is short (<3 hours), resulting in modeled MeSH mixing ratios being primarily driven by oxidation and not by the uncertain boundary layer dynamics or nighttime emission fluxes. During daytime modeled and measured MeSH mixing ratios agreed to within 25 % while DMS mixing ratios were overpredicted by ~50%. One additional potential driver of model overprediction of DMS during daytime is the exclusion of BrO chemistry from the base model due to the lack of observational constraints of BrO at the study site. BrO has been suggested to be an important oxidant of DMS which peaks in concentration in the afternoon (Saiz-Lopez et al., 2006, 2008). A model sensitivity run using an afternoon peak BrO concentration ( $[\text{BrO}]_{\text{max}}$ ) of 1 ppt was performed which brings modeled DMS to within 10 ppt of the observations during daytime but degrades model to observation agreement at night. The  $[\text{BrO}]_{\text{max}}$  of 1 ppt was selected as an intermediate value in the range of measured and modeled BrO in the daytime marine boundary layer, however mean daytime BrO mixing ratios of up to 4 ppt have been observed in some locations (Mahajan et al., 2010; Saiz-Lopez et al., 2004; Wang et al., 2019). Implementing higher BrO mixing ratios in this model would generally serve to decrease modeled DMS and MeSH mixing ratios, especially during daytime. Daytime MeSH mixing ratios are reduced by less than 0.5 ppt in the 1 ppt BrO sensitivity test, as MeSH oxidation is still dominated by OH. Due to the lack of observational constraint on BrO during our study, we elect to exclude BrO chemistry from the model base case used in subsequent calculations. Inclusion of BrO chemistry would have minimal impact on model MeSH as described, and would serve to reduce DMS lifetime, increase the yield of DMSO and MSA from DMS oxidation, and reduce the yield of  $\text{SO}_2$  from DMS oxidation. While there are clear uncertainties in this modelling effort especially during nighttime, the general model ability to reproduce observed DMS and especially MeSH mixing ratios during daytime when we have robust constraints on



the emission flux suggests that the DMS and MeSH oxidation mechanism added to the MCM v3.3.1 in this work is suitably  
410 accurate to provide meaningful information on the oxidative fate of DMS and MeSH.

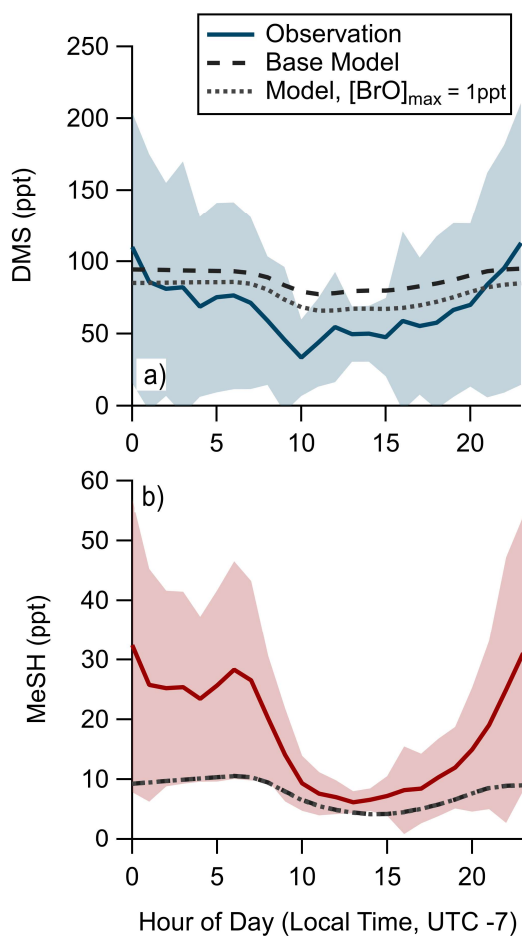


Figure 7. Observed and modeled diel profiles of (a) DMS and (b) MeSH mixing ratios.

### 3.5 Impact of MeSH on Marine Sulfur Dioxide Production

Production of  $\text{SO}_2$  as a function of  $F_{\text{DMS}}$  and  $F_{\text{MeSH}}$  was assessed using the Open Ocean case of the coupled ocean-atmosphere  
415 0-D box model described in Section 2.4.2.2. Chemical box modeling of MeSH emission and gas phase oxidation suggest that  
MeSH contributes significantly to marine boundary layer  $\text{SO}_2$  concentration. For a model case where  $F_{\text{MeSH}}$  is taken to be 0,  
and  $F_{\text{DMS}}$  is taken to be the campaign mean of  $1.1 \text{ ppt m s}^{-1}$ , modeled afternoon (hours 12 to 16) mean  $\text{SO}_2$  mixing ratio is 29.5  
ppt, and the instantaneous  $\text{SO}_2$  production rate ( $P_{\text{SO}_2}$ ) is  $5.8 \text{ ppt h}^{-1}$ . When  $F_{\text{MeSH}}$  is added to the model at the observed campaign  
420 mean of  $0.21 \text{ ppt m s}^{-1}$ , model afternoon mean  $\text{SO}_2$  increases to 46.5 ppt and  $P_{\text{SO}_2}$  increases to  $8.3 \text{ ppt h}^{-1}$ . Model diel profiles  
of  $\text{SO}_2$  mixing ratios and  $P_{\text{SO}_2}$  with and without MeSH emissions are shown in Fig 8. In the campaign mean case MeSH  
emissions contribute 30% of the overall  $\text{SO}_2$  production (or a 43% increase in total  $\text{SO}_2$  production compared to the  $F_{\text{DMS}}$  only  
case). The model yield of  $\text{SO}_2$  from MeSH oxidation was 0.99 which is comparable to an experimentally constrained model

determination of the atmospheric yield of 0.98 (Chen et al., 2021). We include the full MeSH oxidation mechanism for completeness due to its overlap with known DMS chemistry and ease of implementation in the box model. But given our  
425 determined model yield of SO<sub>2</sub> from MeSH of 0.99, and a recently determined yield of 0.98 constrained by laboratory oxidation studies (Chen et al., 2021), future modeling efforts may be justified in simplifying this mechanism by including only a direct MeSH + OH → SO<sub>2</sub> reaction at a yield of 1. Prior efforts to constrain the total SO<sub>2</sub> budget in the marine boundary layer required a unit yield of SO<sub>2</sub> from DMS (Faloona et al., 2009) which stands in contrast to the 40-80% range typically determined in laboratory and modeling studies (Faloona, 2009; Gray et al., 2011). This discrepancy has prompted consideration that other  
430 potential SO<sub>2</sub> precursors might be present which might reduce the yield of SO<sub>2</sub> from DMS needed to close the SO<sub>2</sub> budget (Bandy et al., 2011). Oceanic MeSH emissions as observed in our study are likely one such additional contributor to secondary marine SO<sub>2</sub> which has not been previously considered. Eddy covariance flux measurements of ocean-atmosphere trace gas exchange have generally been limited to a small set of molecules (e.g. DMS, acetone, methanol, acetaldehyde) (Novak and Bertram, 2020). As demonstrated with the MeSH measurements presented here, marine EC flux observations of new molecules  
435 are critical to constrain marine sulfur and volatile organic compound (VOC) budgets. Global spatiotemporal variability of MeSH emission flux magnitude and the ratio of  $F_{\text{DMS}}:F_{\text{MeSH}}$  are both highly uncertain due to the sparsity of ambient observations, which will need to be better constrained through future studies.

Heterogeneous chemistry of the DMS oxidation product HPMTF is not included in our base model case. HPMTF heterogeneous chemistry has been proposed to be a potentially large sink for HPMTF which would reduce SO<sub>2</sub> production  
440 from DMS (Novak et al., 2021; Veres et al., 2020; Vermeuel et al., 2020). These details of HPMTF heterogeneous chemistry do not impact the yield of SO<sub>2</sub> from MeSH described previously but do impact the calculated relative production of SO<sub>2</sub> from MeSH compared to DMS. Inclusion of HPMTF heterogeneous chemistry (at  $\gamma=0.01$  and aerosol surface area of  $48 \mu\text{m}^2 \text{cm}^{-3}$ ) reduces model SO<sub>2</sub> production from DMS to 2.7 ppt h<sup>-1</sup> compared to 5.8 ppt h<sup>-1</sup> in the model base case. In the HPMTF heterogeneous chemistry case MeSH oxidation accounts for 48% of marine SO<sub>2</sub> production. Further details on HPMTF  
445 chemistry are given in SI S5.

We also note that the yield of SO<sub>2</sub> production from MeSH does not have a temperature dependence, unlike DMS, which may result in MeSH being an especially important source of SO<sub>2</sub> in colder high latitude regions. At lower temperatures, the DMS OH-addition reaction pathway becomes more favored, resulting in less efficient production of SO<sub>2</sub> from DMS oxidation as production of highly soluble intermediates begins to dominate compared to at higher temperatures. Model calculations  
450 presented here used the measured diel temperature profile at the SIO pier during this study which had a mean of 293 K.

Modeled daytime  $P_{\text{SO}_2}$  as a function of DMS and MeSH emission flux magnitude are shown in **Fig. 9** with the interquartile range of  $F_{\text{MeSH}}$  and  $F_{\text{DMS}}$  measured SIO pier emission fluxes overlaid as a constraint. These results highlight the potential variability in  $P_{\text{SO}_2}$  in varying regimes of  $F_{\text{DMS}}:F_{\text{MeSH}}$ . Model results were from the base Open Ocean Case described in **Section 2.4.2.2**. Given the potential biological control on  $F_{\text{DMS}}:F_{\text{MeSH}}$ , the temperature dependence of SO<sub>2</sub> yield from DMS, and the  
455 impact of HPMTF heterogeneous chemistry on SO<sub>2</sub> yield from DMS, we expect there may be significant temporal and regional variability in the relative contribution of DMS and MeSH to marine  $P_{\text{SO}_2}$  across the global oceans. This additional SO<sub>2</sub>

production from MeSH will likely contribute to new particle formation and growth through enhanced production of sulfuric acid ( $\text{H}_2\text{SO}_4$ ) with subsequent impacts on CCN abundance in the MBL. Given the newly determined significance of both MeSH emissions and HPMTF heterogeneous chemistry on marine  $\text{SO}_2$  production, a critical reevaluation of the global marine  $\text{SO}_2$  budget is likely warranted.

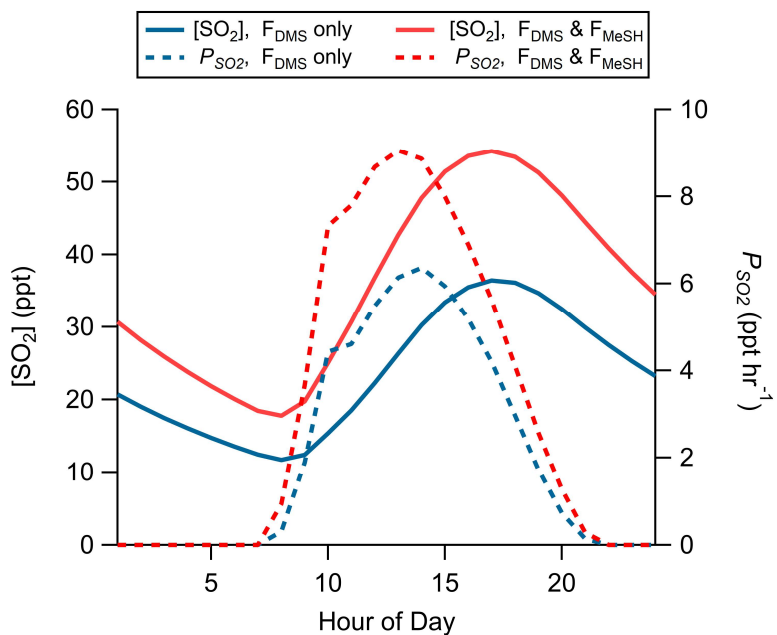
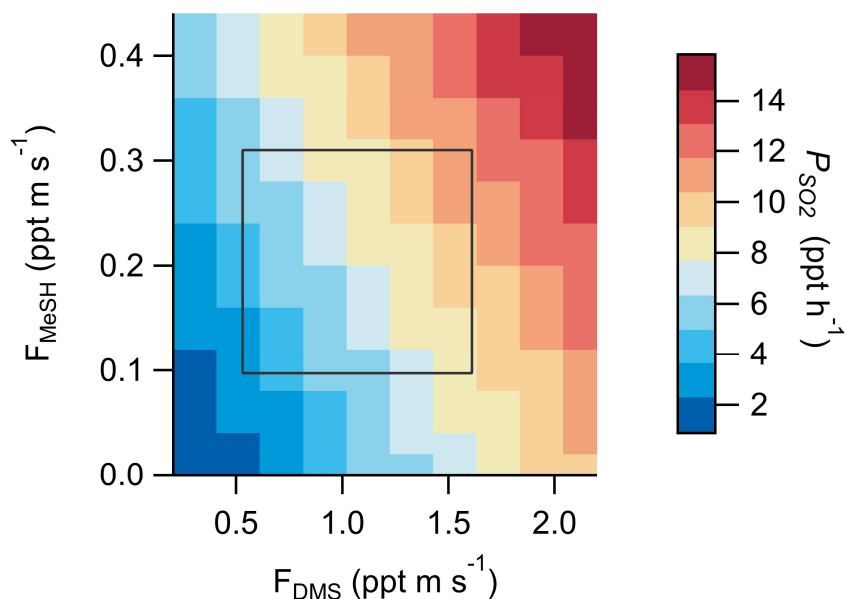


**Figure 8. Modeled diel profiles of  $\text{SO}_2$  mixing ratios and instantaneous  $\text{SO}_2$  production rates ( $P_{\text{SO}_2}$ ) for a model case considering only DMS emissions ( $F_{\text{DMS}}$  only, blue traces) and one including both DMS and MeSH emissions ( $F_{\text{DMS}}$  &  $F_{\text{MeSH}}$ , red traces). Emissions were taken as the measured campaign mean flux of DMS and MeSH.**



465

**Figure 9. Modeled SO<sub>2</sub> production rate ( $P_{SO_2}$ ) in the marine boundary layer as a function of MeSH and DMS emission fluxes. The interquartile range of measured  $F_{DMS}$  and  $F_{MeSH}$  at SIO pier is plotted as a black square.**

### 3.6 Limited observational evidence for other volatile organic sulfur compounds

In addition to DMS and MeSH, several other volatile organic sulfur compounds (VOSCs) have been reported to be significant in the marine atmosphere, either from direct oceanic emissions or gas phase oxidation of precursor species. Recent shipborne observations in the Arabian Sea reported high mixing ratios of dimethyl sulfone (DMSO<sub>2</sub>, 40-120 ppt) and methane sulfonamide (MSAM, 20-50 ppt) downwind of a biologically productive upwelling region (Edtbauer et al., 2020). Reported DMS in the same region was from 100-300 ppt. The authors in that study propose a direct oceanic emission source of MSAM as there is no known gas phase oxidation pathway to produce MSAM from DMS. For our observations at Scripps Pier, both MSAM and DMSO<sub>2</sub> were found to have no observable emission flux above the flux limit of detection at either the standard 3σ LOD threshold or a more relaxed 1σ LOD threshold. Gas phase mixing ratios of MSAM, DMSO, and DMSO<sub>2</sub> were also not found to be significant, with none of those species consistently observed above the 10 s averaging time LOD of 2.4, 7.0, and 9.2 ppt respectively. All determinations of MSAM, DMSO, and DMSO<sub>2</sub> mixing ratio and LOD assume they have the same detection sensitivity as DMS. Our measurements of DMSO and DMSO<sub>2</sub> are consistent with box model calculated mixing ratios which show hourly maxima of 4.9 ppt and <0.1 ppt for DMSO and DMSO<sub>2</sub>, respectively which are both below the instrument LOD. The box model conditions used were the Pier Model Case with the addition of [BrO]<sub>max</sub> of 1 ppt. Oxidation of DMS by BrO favors DMSO and DMSO<sub>2</sub> production and the inclusion of [BrO]<sub>max</sub> of 1 ppt was done as a test of the reasonable upper limit case for DMSO and DMSO<sub>2</sub> production for conditions during this study. DMSO<sub>2</sub> has also been measured at Palmer Station, Antarctica in January to February of 1994 with mean and median mixing ratios of 1.7 and 1.3 ppt respectively (Berresheim, 1998). The higher DMSO<sub>2</sub> mixing ratios observed in that study are likely at least in part due to the

475

485

much lower temperatures (mean 274.5 K), where the DMS + OH addition channel forming DMSO and DMSO<sub>2</sub> is more favored. Dimethyl disulfide (DMDS, CH<sub>3</sub>S<sub>2</sub>CH<sub>3</sub>) was also not consistently observed above the LOD in our measurements.

While a direct oceanic emission source of MSAM to the atmosphere has been proposed (Edtbauer et al., 2020), we did not measure a detectable MSAM emission flux in this study. As noted by Edtbauer et. al. (2020), given the Henry's law constant of MSAM ( $K_H = 3.3 \times 10^4 \text{ M atm}^{-1}$ ), the waterside concentration of MSAM necessary to drive a net emission flux of MSAM to the atmosphere is on the order of 1700 nM. Given that maximum total dissolved organic sulfur (DOS) in ocean surface waters are on the order of 200 nM (Ksionzek et al., 2016), even if all surface ocean DOS was in the form of MSAM, we still would not expect an emission flux of MSAM to the atmosphere. This exercise suggests MSAM may instead be formed through an unknown reaction pathway in the atmosphere which was active in the Arabian Sea but not in our observations at SIO Pier in coastal southern California. Taken together our observations indicate that MSAM, DMSO, and DMSO<sub>2</sub> emission fluxes and mixing ratios were small at the SIO Pier site consistent with model calculations.

This discussion on the lack of observations of other VOSCs only extends to molecules that are detectable with the Vocus PTR instrument, such as DMSO, DMSO<sub>2</sub>, MSAM, and DMDS. For example, it does not include inorganic sulfur containing molecules such as carbonyl sulfide (OCS) and carbon disulfide (CS<sub>2</sub>) which also have a known oceanic source but are not readily detectable by PTR. In particular our measurements do not include the recently observed DMS oxidation product HPMTF which was found to be a globally ubiquitous sulfur reservoir from airborne observations in the marine atmosphere (Veres et al., 2020) and in prior surface observations at the SIO Pier (Vermeuel et al., 2020). HPMTF is not detectable with the Vocus PTR ion chemistry used in this study. HPMTF was previously observed in the summer of 2018 at the SIO Pier site to have a strong diel profile, peaking in the early afternoon with an average daytime mixing ratio of 12.1 pptv (Vermeuel et al., 2020). While observations of HPMTF were made one year prior to the DMS and MeSH observations reported here, it suggests that HPMTF may comprise up to 10-20% of the total daytime VOSC concentration at this site during summer.

#### 4. Conclusions

We present the first direct eddy covariance flux measurement of MeSH emissions from the ocean which show that MeSH emissions account for a mean of 16% ( $F_{\text{MeSH}}/(F_{\text{MeSH}} + F_{\text{DMS}})$ ) of emitted volatile organic sulfur measurable with the Vocus PTR-ToF during this study. DMS and MeSH emission fluxes were correlated with each other ( $R^2 = 0.65$ ), consistent with their shared oceanic source from the degradation of DMSP. Measured  $F_{\text{DMS}}:F_{\text{MeSH}}$  was found to have a weak correlation ( $R^2 = 0.15$ ) with chlorophyll concentrations, which highlights the need for further study of biogeochemical cycling in the ocean surface which may drive significant spatiotemporal variability in  $F_{\text{MeSH}}$ . The atmospheric implications of ocean MeSH emissions were assessed by development of a MeSH oxidation mechanism and incorporation into a coupled ocean-atmosphere 0-dimensional chemical box model. Modeling results show that oxidation of MeSH by OH produces SO<sub>2</sub> at a high yield (~99%) and is an important contributor to SO<sub>2</sub> production in the marine atmosphere, driving an increase in afternoon  $P_{\text{SO}_2}$  of 2.5 ppt hr<sup>-1</sup>, corresponding to 30% of total afternoon SO<sub>2</sub> production rates. In a model case including HPMTF heterogeneous uptake to

aerosols, SO<sub>2</sub> yield from DMS is reduced and MeSH becomes even more important, accounting for 48% of marine SO<sub>2</sub> production. Taken together these results demonstrate that MeSH is an important contributor to volatile sulfur budgets in the marine atmosphere and that further studies are needed to constrain spatiotemporal trends of MeSH emission and oxidation relative to DMS.

**Code and Data Availability.** DMS and MeSH flux and concentration data and associated meteorological data from this study are archived at <http://digital.library.wisc.edu/1793/82383>.

**Author Contributions.** GAN, DBK, and THB designed research. GAN carried out the ambient sampling campaign and analyzed the data. MPV assisted with the ambient deployment. DBK conducted laboratory calibrations and developed sampling methods. CMJ and MPV contributed to model development. THB supervised the project. GAN and THB wrote the paper. All authors reviewed and edited the paper.

**Competing Interests.** Timothy H. Bertram is a member of the editorial board of Atmospheric Chemistry and Physics. The authors have no other competing interests to declare.

**Acknowledgments.** This work was supported by National Science Foundation (NSF) Grant GEO AGS 1829667 and through the National Science Foundation Center for Aerosol Impacts on Chemistry of the Environment (NSF-CAICE) under Grant CHE 1801971.

## References

- Andreae, M. O.: Ocean-atmosphere interactions in the global biogeochemical sulfur cycle, *Mar. Chem.*, 30(C), 1–29, doi:10.1016/0304-4203(90)90059-L, 1990.
- Archer, C. L. and Jacobson, M. Z.: Evaluation of global wind power, *J. Geophys. Res. D Atmos.*, 110(D12), D12110, doi:10.1029/2004JD005462, 2005.
- Bandy, A., Faloon, I. C., Blomquist, B. W., Huebert, B. J., Clarke, A. D., Howell, S. G., Mauldin, R. L., Cantrell, C. A., Hudson, J. G., Heikes, B. G., Merrill, J. T., Wang, Y., O’Sullivan, D. W., Nadler, W. and Davis, D. D.: Pacific Atmospheric Sulfur Experiment (PASE): Dynamics and chemistry of the south Pacific tropical trade wind regime, *J. Atmos. Chem.*, 68(1), 5–25, doi:10.1007/s10874-012-9215-8, 2011.
- Barnes, I., Hjorth, J. and Mihalopoulos, N.: Dimethyl sulfide and dimethyl sulfoxide and their oxidation in the atmosphere, *Chem. Rev.*, 106(3), 940–975, doi:10.1021/cr020529+, 2006.
- Bates, T. S., Charlson, R. J. and Gammon, R. H.: Evidence for the climatic role of marine biogenic sulphur, *Nature*, 329(6137), 319–321, doi:10.1038/329319a0, 1987a.
- Bates, T. S., Cline, J. D., Gammon, R. H. and Kelly-Hansen, S. R.: Regional and seasonal variations in the flux of oceanic dimethylsulfide to the atmosphere, *J. Geophys. Res.*, 92(C3), 2930, doi:10.1029/JC092iC03p02930, 1987b.
- Bates, T. S., Lamb, B. K., Guenther, A., Dignon, J. and Stoiber, R. E.: Sulfur emissions to the atmosphere from natural sources,

- J. Atmos. Chem., 14(1–4), 315–337, doi:10.1007/BF00115242, 1992.
- 550 Berndt, T., Scholz, W., Mentler, B., Fischer, L., Hoffmann, E. H., Tilgner, A., Hyttinen, N., Prisle, N. L., Hansel, A. and Herrmann, H.: Fast peroxy radical isomerization and OH recycling in the reaction of OH radicals with dimethyl sulfide, *J. Phys. Chem. Lett.*, 6478–6483, doi:10.1021/acs.jpcelett.9b02567, 2019.
- Berresheim, H.: Biogenic Sulfur Emissions from the Subantarctic and Antarctic Oceans, *Journa Gecophysical Res.*, 92(D11), 13245–13262, doi:https://doi.org/10.1029/JD092iD11p13245, 1987.
- 555 Berresheim, H.: Measurements of dimethyl sulfide, dimethyl sulfoxide, dimethyl sulfone, and aerosol ions at Palmer Station, Antarctica, *J. Geophys. Res. Atmos.*, doi:10.1029/97JD00695, 1998.
- Bertram, T. H., Kimmel, J. R., Crisp, T. A., Ryder, O. S., Yatavelli, R. L. N., Thornton, J. A., Cubison, M. J., Gonin, M. and Worsnop, D. R.: A field-deployable, chemical ionization time-of-flight mass spectrometer, *Atmos. Meas. Tech.*, 4(7), 1471–1479, doi:10.5194/amt-4-1471-2011, 2011.
- 560 Butkovskaya, N. I. and Setser, D. W.: Product Branching Fractions and Kinetic Isotope Effects for the Reactions of OH and OD Radicals with CH<sub>3</sub>SH and CH<sub>3</sub>SD, *J. Phys. Chem. A*, 103(35), 6921–6929, doi:10.1021/jp9914828, 1999.
- Butkovskaya, N. I. and Setser, D. W.: Reactions of OH and OD radicals with simple thiols and sulfides studied by infrared chemiluminescence of isotopic water products: Reaction OH + CH<sub>3</sub>SH revisited, *Int. J. Chem. Kinet.*, 53(6), 702–715, doi:10.1002/kin.21475, 2021.
- 565 Carpenter, L. J., Archer, S. D. and Beale, R.: Ocean-atmosphere trace gas exchange, *Chem. Soc. Rev.*, 41(19), 6473–6506, doi:10.1039/c2cs35121h, 2012.
- Carslaw, K. S., Lee, L. A., Reddington, C. L., Pringle, K. J., Rap, A., Forster, P. M., Mann, G. W., Spracklen, D. V., Woodhouse, M. T., Regayre, L. A. and Pierce, J. R.: Large contribution of natural aerosols to uncertainty in indirect forcing, *Nature*, 503(7474), 67–71, doi:10.1038/nature12674, 2013.
- 570 Charlson, R. J., Lovelock, J. E., Andreaei, M. O. and Warren, S. G.: Oceanic phytoplankton, atmospheric sulphur, cloud, *Nature*, 330, 1987, 1987.
- Chen, J., Berndt, T., Møller, K. H., Lane, J. R. and Kjaergaard, H. G.: Atmospheric Fate of the CH<sub>3</sub>SOO Radical from the CH<sub>3</sub>S + O<sub>2</sub> Equilibrium, *J. Phys. Chem. A*, 125(40), 8933–8941, doi:10.1021/acs.jpca.1c06900, 2021.
- Clarke, A. D., Varner, J. L., Eisele, F., Mauldin, R. L., Tanner, D. and Litchy, M.: Particle production in the remote marine atmosphere: Cloud outflow and subsidence during ACE 1, *J. Geophys. Res. Atmos.*, 103(D13), 16397–16409, doi:10.1029/97JD02987, 1998.
- 575 Conley, S. A., Faloon, I., Miller, G. H., Lenschow, D. H., Blomquist, B. and Bandy, A.: Closing the dimethyl sulfide budget in the tropical marine boundary layer during the Pacific Atmospheric Sulfur Experiment, *Atmos. Chem. Phys.*, 9(22), 8745–8756, doi:10.5194/acp-9-8745-2009, 2009.
- 580 Edtbauer, A., Stöner, C., Pfannerstill, E. Y., Berasategui, M., Walter, D., Crowley, J. N., Lelieveld, J. and Williams, J.: A new marine biogenic emission: Methane sulfonamide (MSAM), dimethyl sulfide (DMS), and dimethyl sulfone (DMSO<sub>2</sub>) measured in air over the Arabian Sea, *Atmos. Chem. Phys.*, 20(10), 6081–6094, doi:10.5194/acp-20-6081-2020, 2020.

- Faloona, I.: Sulfur processing in the marine atmospheric boundary layer: A review and critical assessment of modeling uncertainties, *Atmos. Environ.*, 43(18), 2841–2854, doi:10.1016/j.atmosenv.2009.02.043, 2009.
- 585 Faloona, I., Lenschow, D. H., Campos, T., Stevens, B., van Zanten, M., Blomquist, B., Thornton, D., Bandy, A. and Gerber, H.: Observations of Entrainment in Eastern Pacific Marine Stratocumulus Using Three Conserved Scalars, *J. Atmos. Sci.*, 62(9), 3268–3285, doi:10.1175/JAS3541.1, 2005.
- Faloona, I., Conley, S. A., Blomquist, B., Clarke, A. D., Kapustin, V., Howell, S., Lenschow, D. H. and Bandy, A. R.: Sulfur dioxide in the tropical marine boundary layer: Dry deposition and heterogeneous oxidation observed during the Pacific atmospheric sulfur experiment, *J. Atmos. Chem.*, 63(1), 13–32, doi:10.1007/s10874-010-9155-0, 2009.
- 590 Foken, T. and Wichura, B.: Tools for quality assessment of surface-based flux measurements, *Agric. For. Meteorol.*, 78(1–2), 83–105, doi:10.1016/0168-1923(95)02248-1, 1996.
- Galí, M., Levasseur, M., Devred, E., Simó, R. and Babin, M.: Sea-surface dimethylsulfide (DMS) concentration from satellite data at global and regional scales, *Biogeosciences*, 15(11), 3497–3519, doi:10.5194/bg-15-3497-2018, 2018.
- 595 Gray, B. A., Wang, Y., Gu, D., Bandy, A., Mauldin, L., Clarke, A., Alexander, B. and Davis, D. D.: Sources, transport, and sinks of SO<sub>2</sub> over the equatorial Pacific during the Pacific Atmospheric Sulfur Experiment, *J. Atmos. Chem.*, 68(1), 27–53, doi:10.1007/s10874-010-9177-7, 2011.
- Hoffmann, E. H., Tilgner, A., Schrödner, R., Bräuer, P., Wolke, R. and Herrmann, H.: An advanced modeling study on the impacts and atmospheric implications of multiphase dimethyl sulfide chemistry, *Proc. Natl. Acad. Sci.*, 113(42), 11776–11781, doi:10.1073/pnas.1606320113, 2016.
- 600 Huebert, B. J., Blomquist, B. W., Hare, J. E., Fairall, C. W., Johnson, J. E. and Bates, T. S.: Measurement of the sea-air DMS flux and transfer velocity using eddy correlation, *Geophys. Res. Lett.*, 31(23), 1–4, doi:10.1029/2004GL021567, 2004.
- Jenkin, M. E., Saunders, S. M. and Pilling, M. J.: The tropospheric degradation of volatile organic compounds: A protocol for mechanism development, *Atmos. Environ.*, 31(1), 81–104, doi:10.1016/S1352-2310(96)00105-7, 1997.
- 605 Kettle, A. J. and Andreae, M. O.: Flux of dimethylsulfide from the oceans: A comparison of updated global oceanic K<sub>w</sub>-e, *J. Geophys. Res. Atmos.*, 105, 26793–26808, 2000.
- Kettle, A. J., Rhee, T. S., Von Hobe, M., Poulton, A., Aiken, J. and Andreae, M. O.: Assessing the flux of different volatile sulfur gases from the ocean to the atmosphere, *J. Geophys. Res. Atmos.*, 106(D11), 12193–12209, doi:10.1029/2000JD900630, 2001.
- 610 Kiene, R. P.: Production of methanethiol from dimethylsulfoniopropionate in marine surface waters, *Mar. Chem.*, 54(1–2), 69–83, doi:10.1016/0304-4203(96)00006-0, 1996.
- Kiene, R. P. and Linn, L. J.: Distribution and turnover of dissolved DMSP and its relationship with bacterial production and dimethylsulfide in the Gulf of Mexico, *Limnol. Oceanogr.*, 45(4), 849–861, doi:10.4319/lo.2000.45.4.0849, 2000a.
- Kiene, R. P. and Linn, L. J.: The fate of dissolved dimethylsulfoniopropionate (DMSP) in seawater: Tracer studies using <sup>35</sup>S-DMSP, *Geochim. Cosmochim. Acta*, 64(16), 2797–2810, doi:10.1016/S0016-7037(00)00399-9, 2000b.
- 615 Kiene, R. P., Linn, L. J. and Bruton, J. A.: New and important roles for DMSP in marine microbial communities, *J. Sea Res.*,



- 43(3–4), 209–224, doi:10.1016/S1385-1101(00)00023-X, 2000.
- Kilgour, D. B., Novak, G. A., Sauer, J. S., Moore, A. N., Dinasquet, J., Amiri, S., Franklin, E. B., Mayer, K., Winter, M., Morris, C. K., Price, T., Malfatti, F., Crocker, D. R., Lee, C., Cappa, C. D., Goldstein, A. H., Prather, K. A. and Bertram, T. H.: Marine gas-phase sulfur emissions during an induced phytoplankton bloom, *Atmos. Chem. Phys.*, 22(2), 1601–1613, doi:10.5194/acp-22-1601-2022, 2022.
- Kim, M. J., Farmer, D. K. and Bertram, T. H.: A controlling role for the air-sea interface in the chemical processing of reactive nitrogen in the coastal marine boundary layer, *Proc. Natl. Acad. Sci. U. S. A.*, 111(11), 3943–3948, doi:10.1073/pnas.1318694111, 2014.
- 625 Kim, M. J., Novak, G. A., Zoerb, M. C., Yang, M., Blomquist, B. W., Huebert, B. J., Cappa, C. D. and Bertram, T. H.: Air-Sea exchange of biogenic volatile organic compounds and the impact on aerosol particle size distributions, *Geophys. Res. Lett.*, 44(8), 3887–3896, doi:10.1002/2017GL072975, 2017.
- Krechmer, J., Lopez-Hilfiker, F., Koss, A., Hutterli, M., Stoerner, C., Deming, B., Kimmel, J., Warneke, C., Holzinger, R., Jayne, J., Worsnop, D., Fuhrer, K., Gonin, M. and De Gouw, J.: Evaluation of a New Reagent-Ion Source and Focusing Ion-Molecule Reactor for Use in Proton-Transfer-Reaction Mass Spectrometry, *Anal. Chem.*, 90(20), 12011–12018, doi:10.1021/acs.analchem.8b02641, 2018.
- 630 Ksionzek, K. B., Lechtenfeld, O. J., McCallister, S. L., Schmitt-Kopplin, P., Geuer, J. K., Geibert, W. and Koch, B. P.: Dissolved organic sulfur in the ocean: Biogeochemistry of a petagram inventory, *Science* (80-. ), 354(6311), 456–459, doi:10.1126/science.aaf7796, 2016.
- 635 Lana, A., Bell, T. G., Simó, R., Vallina, S. M., Ballabrera-Poy, J., Kettle, A. J., Dachs, J., Bopp, L., Saltzman, E. S., Stefels, J., Johnson, J. E. and Liss, P. S.: An updated climatology of surface dimethylsulfide concentrations and emission fluxes in the global ocean, *Global Biogeochem. Cycles*, 25(1), 1–17, doi:10.1029/2010GB003850, 2011.
- Lawson, S. J., Law, C. S., Harvey, M. J., Bell, T. G., Walker, C. F., De Bruyn, W. J. and Saltzman, E. S.: Methanethiol, dimethyl sulfide and acetone over biologically productive waters in the southwest Pacific Ocean, *Atmos. Chem. Phys.*, 20(5), 3061–3078, doi:10.5194/acp-20-3061-2020, 2020.
- 640 Leck, C. and Rodhe, H.: Emissions of marine biogenic sulfur to the atmosphere of northern Europe, *J. Atmos. Chem.*, 12(1), 63–86, doi:10.1007/BF00053934, 1991.
- Lee, C. L. and Brimblecombe, P.: Anthropogenic contributions to global carbonyl sulfide, carbon disulfide and organosulfides fluxes, *Earth-Science Rev.*, 160, 1–18, doi:10.1016/j.earscirev.2016.06.005, 2016.
- 645 Liss, P. S. and Slater, P. G.: Flux of gases across the Air-Sea interface, *Nature*, 247(5438), 181–184, doi:10.1038/247181a0, 1974.
- Lucas, D. D.: Mechanistic studies of dimethylsulfide oxidation products using an observationally constrained model, *J. Geophys. Res.*, 107(D14), 1–26, doi:10.1029/2001jd000843, 2002.
- Mahajan, A. S., Plane, J. M. C., Oetjen, H., Mendes, L., Saunders, R. W., Saiz-Lopez, A., Jones, C. E., Carpenter, L. J. and 650 McFiggans, G. B.: Measurement and modelling of tropospheric reactive halogen species over the tropical Atlantic Ocean,

- Atmos. Chem. Phys., 10(10), 4611–4624, doi:10.5194/acp-10-4611-2010, 2010.
- Mai, T. V. T., Nguyen, H. T. and Huynh, L. K.: Kinetics of hydrogen abstraction from CH<sub>3</sub>SH by OH radicals: An ab initio RRKM-based master equation study, Atmos. Environ., 242(April), 117833, doi:10.1016/j.atmosenv.2020.117833, 2020.
- Marandino, C. A., De Bruyn, W. J., Miller, S. D. and Saltzman, E. S.: Eddy correlation measurement of the air/sea flux of dimethylsulfide over the North Pacific Ocean, J. Geophys. Res. Atmos., 112(3), 1–12, doi:10.1029/2006JD007293, 2007.
- 655 Mardyukov, A. and Schreiner, P. R.: Atmospherically Relevant Radicals Derived from the Oxidation of Dimethyl Sulfide, Acc. Chem. Res., 51(2), 475–483, doi:10.1021/acs.accounts.7b00536, 2018.
- Mauder, M., Cuntz, M., Drüe, C., Graf, A., Rebmann, C., Schmid, H. P., Schmidt, M. and Steinbrecher, R.: A strategy for quality and uncertainty assessment of long-term eddy-covariance measurements, Agric. For. Meteorol., 169, 122–135, doi:10.1016/j.agrformet.2012.09.006, 2013.
- 660 Novak, G., Vermeuel, M. and Bertram, T.: Simultaneous Detection of Ozone and Nitrogen Dioxide by Oxygen Anion Chemical Ionization Mass Spectrometry: A Fast Time Response Sensor Suitable for Eddy Covariance Measurements, Atmos. Meas. Tech., 13, 1887–1907, doi:10.5194/amt-13-1887-2020, 2020.
- Novak, G. A. and Bertram, T. H.: Reactive VOC Production from Photochemical and Heterogeneous Reactions Occurring at the Air-Ocean Interface, Acc. Chem. Res., doi:10.1021/acs.accounts.0c00095, 2020.
- 665 Novak, G. A., Fite, C. H., Holmes, C. D., Veres, P. R., Neuman, J. A., Faloon, I., Thornton, J. A., Wolfe, G. M., Vermeuel, M. P., Jernigan, C. M., Peischl, J., Ryerson, T. B., Thompson, C. R., Bourgeois, I., Warneke, C., Gkatzelis, G. I., Coggon, M. M., Sekimoto, K., Bui, T. P., Dean-Day, J., Diskin, G. S., DiGangi, J. P., Nowak, J. B., Moore, R. H., Wiggins, E. B., Winstead, E. L., Robinson, C., Thornhill, K. L., Sanchez, K. J., Hall, S. R., Ullmann, K., Dollner, M., Weinzierl, B., Blake, D. R. and Bertram, T. H.: Rapid cloud removal of dimethyl sulfide oxidation products limits SO<sub>2</sub> and cloud condensation nuclei production in the marine atmosphere, Proc. Natl. Acad. Sci., 118(42), e2110472118, doi:10.1073/pnas.2110472118, 2021.
- Perraud, V., Meinardi, S., Blake, D. R. and Finlayson-Pitts, B. J.: Challenges associated with the sampling and analysis of organosulfur compounds in air using real-time PTR-ToF-MS and offline GC-FID, Atmos. Meas. Tech., 9(3), 1325–1340, doi:10.5194/amt-9-1325-2016, 2016.
- 675 Porter, J. G., De Bruyn, W. and Saltzman, E. S.: Eddy flux measurements of sulfur dioxide deposition to the sea surface, Atmos. Chem. Phys., 18(20), 15291–15305, doi:10.5194/acp-18-15291-2018, 2018.
- Quinn, P. K. and Bates, T. S.: The case against climate regulation via oceanic phytoplankton sulphur emissions, Nature, 480(7375), 51–56, doi:10.1038/nature10580, 2011.
- Riedel, T. P., Wolfe, G. M., Danas, K. T., Gilman, J. B., Kuster, W. C., Bon, D. M., Vlasenko, A., Williams, E. J., Lerner, B. M., Veres, P. R., Roberts, J. M., Holloway, J. S., Lefer, B., Brown, S. S. and Thornton, J. A.: An mcm modeling study of nitryl chloride (ClNO<sub>2</sub>) impacts on oxidation, ozone production and nitrogen oxide partitioning in polluted continental outflow, Atmos. Chem. Phys., 14(8), 3789–3800, doi:10.5194/acp-14-3789-2014, 2014.
- 680 Saiz-Lopez, A., Plane, J. M. C. and Shillito, J. A.: Bromine oxide in the mid-latitude marine boundary layer, Geophys. Res. Lett., 31(3), 4–7, doi:10.1029/2003GL018956, 2004.

- 685 Saiz-Lopez, A., Shillito, J. A., Coe, H. and Plane, J. M. C.: Measurements and modelling of I<sub>2</sub>, IO, OIO, BrO and NO<sub>3</sub> in the mid-latitude marine boundary layer, *Atmos. Chem. Phys.*, 6(6), 1513–1528, doi:10.5194/acp-6-1513-2006, 2006.
- Saiz-Lopez, A., Plane, J. M. C., Mahajan, A. S., Anderson, P. S., Bauguitte, S. J. B., Jones, A. E., Roscoe, H. K., Salmon, R. A., Bloss, W. J., Lee, J. D. and Heard, D. E.: On the vertical distribution of boundary layer halogens over coastal Antarctica: Implications for O<sub>3</sub>, HO<sub>x</sub>, NO<sub>x</sub> and the Hg lifetime, *Atmos. Chem. Phys.*, 8(4), 887–900, doi:10.5194/acp-8-887-2008, 2008.
- 690 Saunders, S. M., Jenkin, M. E., Derwent, R. G. and Pilling, M. J.: Protocol for the development of the Master Chemical Mechanism, MCM v3 (Part A): Tropospheric degradation of non-aromatic volatile organic compounds, *Atmos. Chem. Phys.*, 3(1), 161–180, doi:10.5194/acp-3-161-2003, 2003.
- Schobesberger, S., Junninen, H., Bianchi, F., Lonn, G., Ehn, M., Lehtipalo, K., Dommen, J., Ehrhart, S., Ortega, I. K., Franchin, A., Nieminen, T., Riccobono, F., Hutterli, M., Duplissy, J., Almeida, J., Amorim, A., Breitenlechner, M., Downard, A. J.,
- 695 Dunne, E. M., Flagan, R. C., Kajos, M., Keskinen, H., Kirkby, J., Kupc, A., Kurten, A., Kurten, T., Laaksonen, A., Mathot, S., Onnela, A., Praplan, A. P., Rondo, L., Santos, F. D., Schallhart, S., Schnitzhofer, R., Sipila, M., Tome, A., Tsagkogeorgas, G., Vehkamäki, H., Wimmer, D., Baltensperger, U., Carslaw, K. S., Curtius, J., Hansel, A., Petaja, T., Kulmala, M., Donahue, N. M. and Worsnop, D. R.: Molecular understanding of atmospheric particle formation from sulfuric acid and large oxidized organic molecules, *Proc Natl Acad Sci U S A*, 110(43), 17223–17228, doi:10.1073/pnas.1306973110, 2013.
- 700 Sciare, J., Mihalopoulos, N. and Dentener, F. J.: Interannual variability of atmospheric dimethylsulfide in the southern Indian Ocean, *J. Geophys. Res. Atmos.*, 105(D21), 26369–26377, doi:10.1029/2000JD900236, 2000.
- Sipila, M., Berndt, T., Petaja, T., Brus, D., Vanhanen, J., Stratmann, F., Patokoski, J., Mauldin, R. L., Hyvärinen, A. P., Lihavainen, H. and Kulmala, M.: The role of sulfuric acid in atmospheric nucleation, *Science* (80-. ), 327(5970), 1243–1246, doi:10.1126/science.1180315, 2010.
- 705 Stull, R. B.: *An Introduction to Boundary Layer Meteorology.*, 1988.
- Sun, J., Todd, J. D., Thrash, J. C., Qian, Y., Qian, M. C., Temperton, B., Guo, J., Fowler, E. K., Aldrich, J. T., Nicora, C. D., Lipton, M. S., Smith, R. D., De Leenheer, P., Payne, S. H., Johnston, A. W. B., Davie-Martin, C. L., Halsey, K. H. and Giovannoni, S. J.: The abundant marine bacterium *Pelagibacter* simultaneously catabolizes dimethylsulfoniopropionate to the gases dimethyl sulfide and methanethiol, *Nat. Microbiol.*, 1(8), 6–11, doi:10.1038/nmicrobiol.2016.65, 2016.
- 710 Tyndall, G. S. and Ravishankara, A. R.: Kinetics of the reaction of the methylthio radical with ozone at 298 K, *J. Phys. Chem.*, 93(12), 4707–4710, doi:10.1021/j100349a006, 1989.
- Tyndall, G. S. and Ravishankara, A. R.: Atmospheric oxidation of reduced sulfur species, *Int. J. Chem. Kinet.*, 23(6), 483–527, doi:10.1002/kin.550230604, 1991.
- Veres, P. R., Andrew Neuman, J., Bertram, T. H., Assaf, E., Wolfe, G. M., Williamson, C. J., Weinzierl, B., Tilmes, S.,
- 715 Thompson, C. R., Thames, A. B., Schroder, J. C., Saiz-Lopez, A., Rollins, A. W., Roberts, J. M., Price, D., Peischl, J., Nault, B. A., Møller, K. H., Miller, D. O., Meinardi, S., Li, Q., Lamarque, J.-F. F., Kupc, A., Kjaergaard, H. G., Kinnison, D., Jimenez, J. L., Jernigan, C. M., Hornbrook, R. S., Hills, A., Dollner, M., Day, D. A., Cuevas, C. A., Campuzano-Jost, P., Burkholder, J., Paul Bui, T., Brune, W. H., Brown, S. S., Brock, C. A., Bourgeois, I., Blake, D. R., Apel, E. C., Ryerson, T. B., Neuman,

- J. A., Bertram, T. H., Assaf, E., Wolfe, G. M., Williamson, C. J., Weinzierl, B., Tilmes, S., Thompson, C. R., Thames, A. B.,  
720 Schroder, J. C., Saiz-Lopez, A., Rollins, A. W., Roberts, J. M., Price, D., Peischl, J., Nault, B. A., Möller, K. H., Miller, D. O.,  
Meinardi, S., Li, Q., Lamarque, J.-F. F., Kupc, A., Kjaergaard, H. G., Kinnison, D., Jimenez, J. L., Jernigan, C. M., Hornbrook,  
R. S., Hills, A., Dollner, M., Day, D. A., Cuevas, C. A., Campuzano-Jost, P., Burkholder, J., Bui, T. P., Brune, W. H., Brown,  
S. S., Brock, C. A., Bourgeois, I., Blake, D. R., Apel, E. C. and Ryerson, T. B.: Global airborne sampling reveals a previously  
725 unobserved dimethyl sulfide oxidation mechanism in the marine atmosphere, *Proc. Natl. Acad. Sci. U. S. A.*, 117(9), 4505–  
4510, doi:10.1073/pnas.1919344117, 2020.
- Vermeuel, M. P., Novak, G. A., Jernigan, C. M. and Bertram, T. H.: Diel profile of hydroperoxymethyl thioformate: evidence  
for surface deposition and multiphase chemistry, *Environ. Sci. Technol.*, 54(19), 12521–12529, doi:10.1021/acs.est.0c04323,  
2020.
- Wang, X., Jacob, D. J., Eastham, S. D., Sulprizio, M. P., Zhu, L., Chen, Q., Alexander, B., Sherwen, T., Evans, M. J., Lee, B.  
730 H., Haskins, J. D., Lopez-Hilfiker, F. D., Thornton, J. A., Huey, G. L. and Liao, H.: The role of chlorine in global tropospheric  
chemistry, *Atmos. Chem. Phys.*, 19(6), 3981–4003, doi:10.5194/acp-19-3981-2019, 2019.
- Wei, J., Tang, G., Zhu, X., Wang, L., Liu, Z., Cheng, M., Münkel, C., Li, X. and Wang, Y.: Thermal internal boundary layer  
and its effects on air pollutants during summer in a coastal city in North China, *J. Environ. Sci. (China)*, 70, 37–44,  
doi:10.1016/j.jes.2017.11.006, 2018.
- 735 Wilczak, J. M., Oncley, S. P. and Stage, S. A.: Sonic anemometer tilt correction algorithms, *Boundary-Layer Meteorol.*, 99(1),  
127–150, doi:10.1023/a:1018966204465, 2001.
- Williams, T. L., Adams, N. G. and Babcock, L. M.: Selected ion flow tube studies of  $\text{H}_3\text{O}^+(\text{H}_2\text{O})_0,1$  reactions with sulfides  
and thiols, *Int. J. Mass Spectrom. Ion Process.*, 172(1–2), 149–159, doi:10.1016/s0168-1176(97)00081-5, 1998.
- Wolfe, G. M., Marvin, M. R., Roberts, S. J., Travis, K. R. and Liao, J.: The framework for 0-D atmospheric modeling (F0AM)  
740 v3.1, *Geosci. Model Dev.*, 9(9), 3309–3319, doi:10.5194/gmd-9-3309-2016, 2016.
- Wright, D.: Oceanographic data collected from station Scripps Pier in the Coastal Waters of California by Southern California  
Coastal Ocean Observing System (SCCOOS) at Scripps Institution of Oceanography (SIO) and assembled by Southern  
California Coastal Ocean Obser, [online] Available from: <https://accession.nodc.noaa.gov/0157035>, 2016.
- Wu, R., Wang, S. and Wang, L.: New mechanism for the atmospheric oxidation of dimethyl sulfide. The importance of  
745 intramolecular hydrogen shift in a  $\text{CH}_3\text{SCH}_2\text{OO}$  radical, *J. Phys. Chem. A*, 119(1), 112–117, doi:10.1021/jp511616j, 2015.
- Yoch, D. C.: Dimethylsulfoniopropionate: Its sources, role in the marine food web, and biological degradation to  
dimethylsulfide, *Appl. Environ. Microbiol.*, 68(12), 5804–5815, doi:10.1128/AEM.68.12.5804-5815.2002, 2002.